Flexural Strengthening of Reinforced Concrete Beams Using Carbon Fiber Reinforced Composites

by

Regan Mechelle Bramblett, B.S.Arch.E.

Thesis

Presented to the Faculty of the Graduate School of

The University of Texas at Austin

in Partial Fulfillment

of the Requirements

for the Degree of

Master of Science in Engineering

The University of Texas at Austin

August 2000

Flexural Strengthening of Reinforced Concrete Beams Using Carbon Fiber Reinforced Composites

Approved by
Supervising Committee:

_____

_____

Dedication

To my family.

Acknowledgements

I would like to thank my supervising professors, Dr. Michael E. Kreger and Dr. Sharon L. Wood, who patiently supported me throughout the year of testing and writing. I am also very grateful to my friend, Sergio Breña, who taught me how to pour concrete and design concrete beams strengthened with composites. It was an honor to learn from their experiences.

I would also like to thank Janna Renfro, Nicole Garcia, and the lab technical staff for helping with all the laborious tasks involved with large scale testing.

The project was sponsored the Texas Department of Transportation and was overseen by Richard Wilkison and Mark Steves. A special thanks goes to TxDot for sponsoring my graduate education.

I also greatly appreciate the generosity of Master Builders, Mitsubishi, Fyfe, and Sika for the donation of materials for testing.

Most of all, I thank my family for supporting my endeavors through the years. Without their love and encouragement, I would not have accomplished so much.

August 18, 2000

Abstract

Flexural Strengthening of Reinforced Concrete Beams Using Carbon Fiber Reinforced Composites

Regan Mechelle Bramblett, M.S.E.

The University of Texas at Austin, 2000

Supervisor: Michael E. Kreger

The Texas Department of Transportation has estimated that 18,000 bridges in use in the state were designed for loads less than today's standards. Some heavier trucks are restricted from passing over these bridges in order to prevent damage from overloading. One solution to this problem is to strengthen the bridges using carbon fiber composites. The objective of this thesis is to develop a strengthening method by investigating the behavior of reinforced concrete beams with externally applied carbon fiber composite materials. Twenty beams were tested monotonically to failure, which was characterized by composite debonding or composite rupture. The results were used for the design and testing of full-scale bridge sections that were part of a second phase of the research project. Results may eventually be implemented on bridges throughout Texas.

Table of Contents

List of Tables

List of Figures

Chapter 1: Introduction

1.1 Research Motivation

Current AASHTO Standard Specifications for Highway Bridges require that new bridge structures be designed to support at least an HS-20 truck load like that illustrated in Figure 1.1 (AASHTO, 1996). Many flat slab, pan joist, and T-beam concrete bridges were constructed in Texas between the 1930's and 1950's for H-10, H-15 and H-20 loadings (Figure 1.2). The Texas Department of Transportation, herein referred to as TxDOT, has estimated that 18,000 bridges in use in the state were designed for less than HS-20 loading criteria (BRINSAP, Dec 1998). Because standard design live loads have increased over the years, many bridges in the state have restrictions on the amount of live load, or truck size, that can pass over the bridge. Bridges with live load restrictions are posted for use only by trucks that meet the acceptable live load criteria. Load posting makes it difficult to route trucks across the state, so strengthening deficient bridges may be an attractive alternative to load posting. In addition, road usage has increased over the years, which has created a demand for widening some bridges. According to TxDOT standards, a bridge must satisfy HS-20 loading criteria in order to be a candidate for widening.

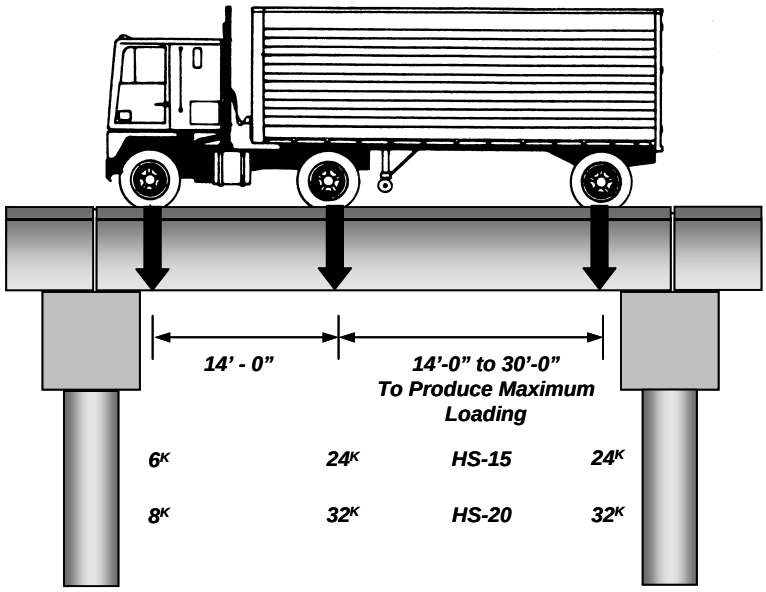

Figure 1.1: Loading Criteria for Standard HS Truck (AASHTO, 1996)

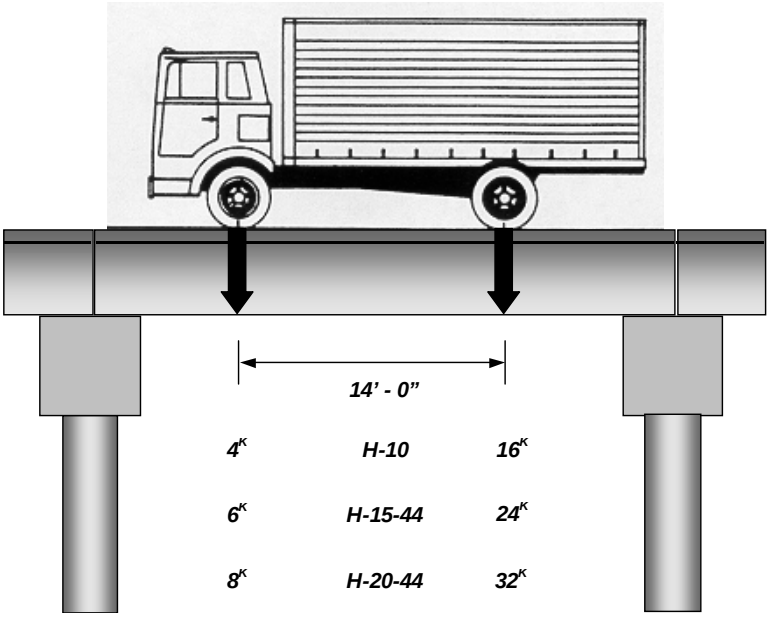

Figure 1.2: Loading Criteria for Standard H Truck (AASHTO, 1996)

As mentioned previously, many bridges are currently load posted to protect against overloads. However, it is common knowledge in the bridge design profession that these bridges are often subjected to overloads from the agricultural trucking industry and concrete industry (BRINSAP, 1997). For example, TxDOT bridge engineers are aware of logging trucks weighing as much as 140 kips using bridges posted for H-15 loading which permits a total two-axle load of 30 kips. It is likely that these violations are accelerating bridge deterioration, and clearly TxDOT engineers are in need of a solution to this problem. Because load posting will not prevent overloaded vehicles from causing damage to bridges with insufficient strength, strengthening may be the best long-term solution.

1.2 JUSTIFICATION FOR STUDYING COMPOSITE MATERIALS

There are many options available for increasing the capacity of existing bridges, such as attaching steel plates to existing girders, adding structural concrete, or completely replacing the bridges. The different methods available for increasing the capacity of short-span, off-system (non-interstate highway) bridges, where flexural strength is deficient, are illustrated schematically in Figure 1.3 for rectangular reinforced concrete beams like those used in this study. Composite fiber systems were chosen in lieu of more traditional methods for the reasons that follow.

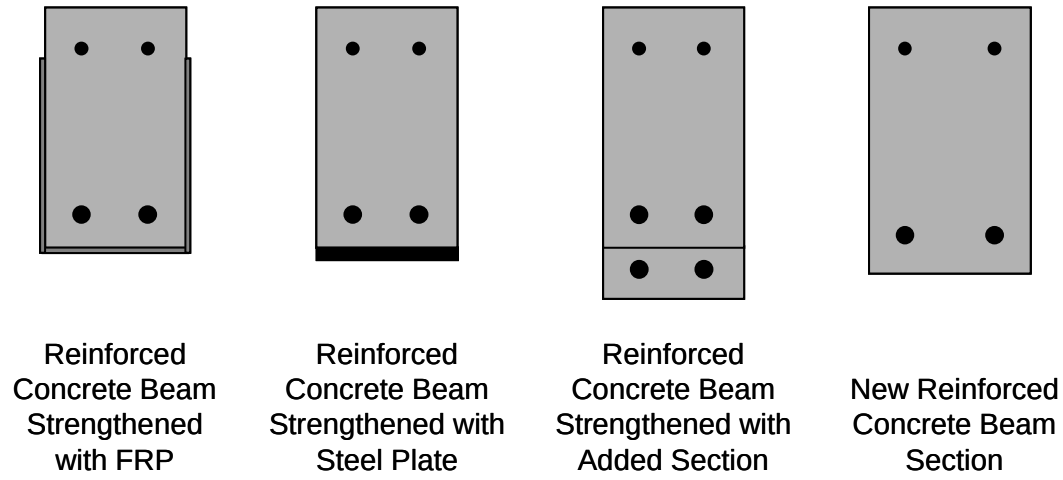

Figure 1.3: Methods for Increasing the Capacity of Existing Concrete Beams

In the past, bridges have been renovated with steel plates anchored to the extreme tension fibers of concrete beams. Because a large amount of material may be required to achieve the appropriate strength level, the steel plates will likely be too heavy to lift without the assistance of a crane or other heavy equipment. In addition, steel plates will add extra dead load to an existing bridge. Because the bridge may cross over a roadway, this construction procedure could result in the roadway being out of service during the strengthening process. There is also the concern that the steel plate will corrode when exposed to weather or deicing chemicals, leading to reduction in plate section, or corrosion will occur between the steel plate and concrete surface (Meier, 1995), resulting in expansion forces between the concrete and steel.

Another method for strengthening existing girders is the addition of steel reinforcement and concrete to the extreme tension fibers of girders. This method also adds dead load and reduces clearance beneath bridges.

There is always the option to replace an existing bridge with a new, stronger structure. In some cases, this may be the most economical solution if labor costs are low. For some cases this may not be an option because of the historical significance of the structure.

Composite systems are lightweight, thin, easy to install, and quite strong. Substantially less material is required to develop the same strength as adding steel plates or reinforced concrete to a section. Material costs for a given required strength are significantly higher than for materials used in traditional strengthening methods, but sufficient time can be saved during construction. The savings in labor costs can offset additional material costs associated with the composite materials (Bassett, 1997). The major drawback to using composites for strengthening is the limited amount of research that has been performed related to attaching composites to reinforced concrete members. Design engineers generally do not have access to guidelines for design and usage of composite materials. Specialized companies with an engineering staff typically have been responsible for the design and application of composites for strengthening of structures. Figures 1.4 and 1.5 show examples of recently strengthened structures using CFRP's for flexural and shear strength enhancement.

Figure 1.4: CFRP Application (Master Builder's, 1998)

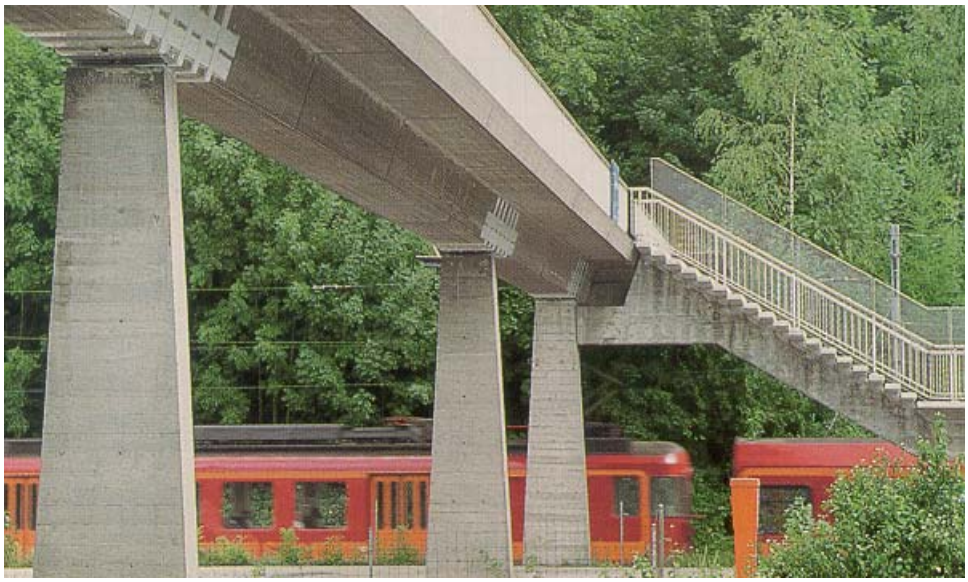

Figure 1.5: CFRP Flexural and Shear Strengthening (Sika, 1999)

1.3 RESEARCH OBJECTIVE

The objective of this thesis was to develop methods for reliably attaching carbon fiber composites to reinforced concrete beams for the purpose of increasing flexural strength, and to develop recommendations for estimating the capacity of the strengthened beams. The results were used in the design of strengthened full-scale beam tests, and eventually may be implemented for use in designing CFRP strengthening schemes for existing bridges. Phase I of the overall research program, described herein, investigated the behavior of reinforced concrete beams with four types of commercially available carbon fiber composite materials applied using different configurations. Recommendations for attaching CFRP to the beams and for calculating the capacity of the strengthened members were developed from the test results.

1.4 SCOPE

Chapter 2 describes the analytical model developed to estimate the flexural capacity of rectangular reinforced concrete beam sections strengthened with carbon fiber composites. Chapter 3 presents a description of the experimental program, and Chapter 4 evaluates the test results. A summary of the testing program and recommendations are presented in Chapter 5.

Chapter 2: Analytical Model used to Estimate the Flexural Capacity of Strengthened Cross Sections

2.1 OBJECTIVE

The purpose of this chapter is to present the analytical model used to estimate the capacity of the reinforced concrete specimens tested during this phase of the research project. However, this procedure is not intended to be used for design because important issues related to bond and anchorage of the composite material to the concrete are not included explicitly in the model.

2.2 ASSUMPTIONS

In order to develop a model for estimating flexural capacity of rectangular, reinforced concrete beams strengthened using CFRP composites, the following simplifying assumptions were made:

1) The composite is bonded perfectly to the concrete surface,
2) Plane sections remain plane, and
3) Loads carried by the reinforced concrete member at the time that the CFRP composites are installed are significantly lower than the yield load; however, the reinforced concrete member may be cracked.

2.3 IDEALIZED MATERIAL BEHAVIOR

2.3.1 Composite Material

The composite is idealized as a linear-elastic material (Figure 2.1). Rupture strains reported by the manufacturers typically range from 0.7% to 2.2% (Cape Composites Incorporated, 2000). The manufacturer supplies critical

composite parameters, such as rupture strain, that are needed for design of strengthened beams.

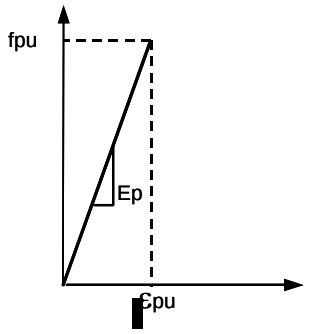

Figure 2.1: Idealized Stress-Strain Relationship for Composite Material

2.3.2 Reinforcing Steel

The stress-strain relationship for steel reinforcement is idealized by a tri-linear relationship as shown in Figure 2.2. The tri-linear model accounts for yielding and strain hardening. Ultimate stress and strain were not specified because rupture of the tensile steel reinforcement was not anticipated during testing.

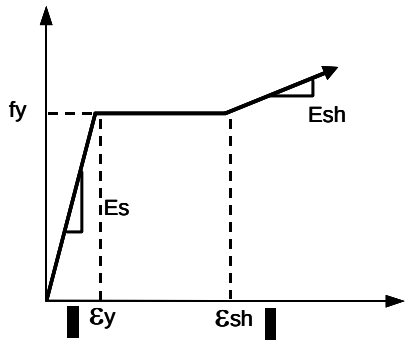

Figure 2.2: Idealized Stress-Strain Relationship for Steel Reinforcement

2.3.3 Concrete

The modified Hognestad model (1951) shown in Figure 2.3 was chosen to describe the stress-strain behavior of concrete in compression. The rectangular stress block typically used in design and recommended by ACI Committee 318 (1999) for use in flexural strength calculations cannot be used to determine the capacity of a strengthened cross section. The rectangular stress block is only valid when the extreme compression fiber reaches the crushing strain. For some of the strengthened beams, the extreme compression fiber strain will be less than the crushing strain when the composite material ruptures. Therefore, the nonlinear relationship between stress and strain in the concrete must be considered explicitly in this procedure. The tensile strength of the concrete was ignored.

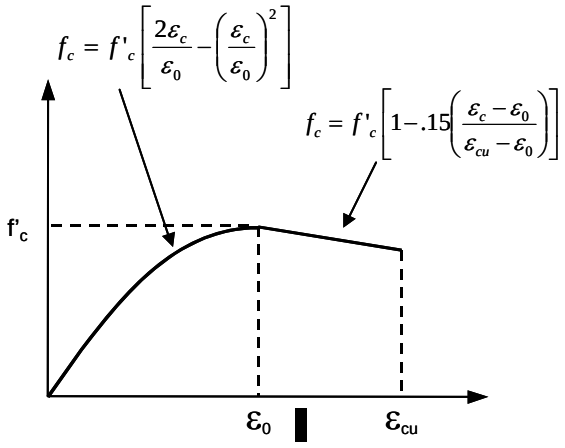

Figure 2.3: Idealized Stress-Strain Relationship for Concrete in Compression

2.4 PROCEDURE USED TO CALCULATE THE FLEXURAL CAPACITY OF STRENGTHENED BEAMS

The failure condition for a reinforced concrete beam strengthened using CFRP composites can be defined by crushing of the concrete or rupture of the composite. The actual failure mode is determined by the area of composite attached to the cross section and the shear stress at which the composites debond from the surface of the concrete. As indicated in Section 2.2, perfect bond between the composites and the concrete was assumed in the analytical model. Therefore, the area of the composite will determine the mode of failure in this analysis.

An approach similar to that used for reinforced concrete members will be used to determine the mode of failure in the strengthened cross sections. The area of composite corresponding to simultaneous crushing of the concrete and rupture of the composite will be defined as the balanced strain condition. When a smaller area of composite is attached to the cross section, failure will be controlled by rupture of the composite. If a larger area of composite is used, failure will be controlled by crushing of the concrete.

The area of composite material corresponding to balanced strain conditions is described in Section 2.4.1. Analysis procedures for cross sections controlled by crushing of the concrete are described in Section 2.4.2, and procedures for cross sections controlled by rupture of the composites are described in Section 2.4.3.

2.4.1 Calculation of Composite Material Area Corresponding with Balanced-Strain Condition

Distributions of strain and stress corresponding to balanced strain conditions are shown in Figure 2.4. The following procedures may be used to determine the corresponding area of composite material.

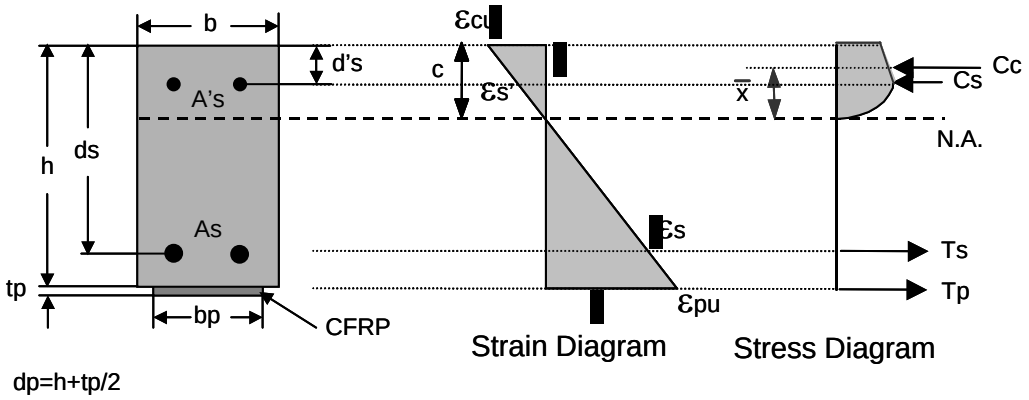

Figure 2.4: Stress and Strain Diagrams for Balanced-Strain Condition

1) Assume $\varepsilon_c = \varepsilon_{cu}$, $\varepsilon_p = \varepsilon_{pu} = \dfrac{f_{pu}}{E_p}$.

2) From strain compatibility, solve for c, ε_s' and ε_s.

$$c = \frac{\varepsilon_{cu} d_p}{(\varepsilon_{cu} + \varepsilon_{pu})} \qquad (2\text{-}1)$$

$$\varepsilon_s = \frac{\varepsilon_{pu}(d_s - c)}{(d_p - c)} \qquad (2\text{-}2)$$

$$\varepsilon_s' = \frac{\varepsilon_c (c - d')}{c} \qquad (2\text{-}3)$$

3) Calculate steel stresses f_s and f_s'.

$$\begin{aligned}
&\text{If } \varepsilon_s \le \varepsilon_y, \text{ then } f_s = \varepsilon_s E_s \\
&\text{If } \varepsilon_y < \varepsilon_s \le \varepsilon_{\text{sh}}, \text{ then } f_s = f_y \\
&\text{If } \varepsilon_s \ge \varepsilon_{sh}, \text{ then } f_s = f_y + (\varepsilon_s - \varepsilon_{sh}) * E_{sh} \\
&f_s' = \varepsilon_s' E_s
\end{aligned} \qquad (2\text{-}4)$$

4) Calculate the resultant concrete compression force. Use modified Hognestad model shown in Figure 2.3 for the concrete stress-strain relationship.

$$C_c = \int_0^c f_c b dy \qquad (2\text{-}5)$$

5) Compute tension and compression forces in steel.

$$\begin{aligned}
C_s &= A_s' f_s' \\
T_s &= A_s f_s
\end{aligned} \qquad (2\text{-}6)$$

6) From equilibrium, solve for T_p.

$$T_p = C_c + C_s - T_s \qquad (2\text{-}7)$$

7) Calculate area of composite required for balanced strain condition.

$$A_{p,b} = \frac{T_p}{f_{pu}} \qquad (2\text{-}8)$$

8) Determine which material controls failure.

$$\begin{aligned}
&\text{If } A_p \le A_{p,b}, \text{ then composite rupture controls computed capacity.} \\
&\text{If } A_p > A_{p,b}, \text{ then concrete crushing controls computed capacity.}
\end{aligned} \qquad (2\text{-}9)$$

2.4.2 Calculation of Flexural Capacity for Concrete-Controlled Failure

Distributions of strain and stress corresponding to concrete-controlled failure conditions are shown in Figure 2.5. The following procedures may be used to determine the corresponding flexural capacity of the strengthened cross-section.

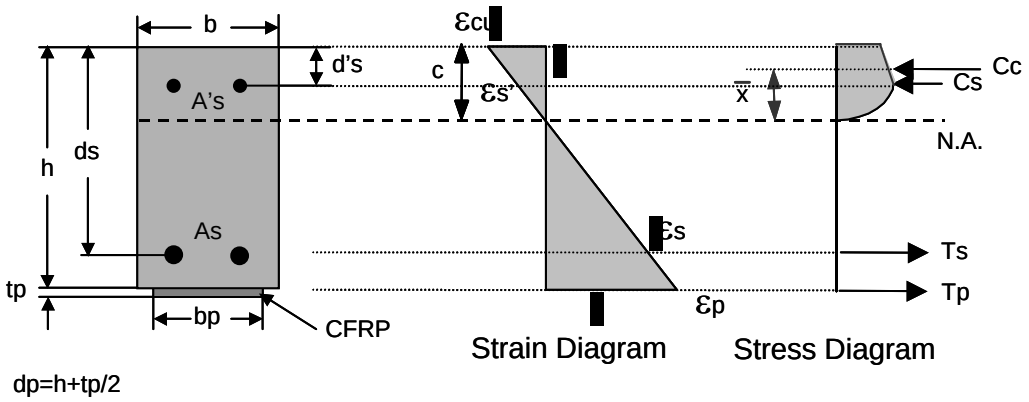

Figure 2.5: Stress and Strain Diagrams for Concrete-Controlled Failure

1) $\varepsilon_c = \varepsilon_{cu}$

2) Assume c, then from strain compatibility compute ε_p, ε_s' and ε_s.

$$\varepsilon_p = \frac{\varepsilon_{cu}(d_p - c)}{c} \qquad (2\text{-}10)$$

$$\varepsilon_s = \frac{\varepsilon_{cu}(d_s - c)}{c} \qquad (2\text{-}11)$$

$$\varepsilon_s^{'} = \frac{\varepsilon_{cu}(c - d')}{c} \qquad (2\text{-}12)$$

3) Calculate steel and composite stresses.

$$\begin{aligned}
&\text{If } \varepsilon_s \le \varepsilon_y, \text{ then } f_s = \varepsilon_s E_s \\
&\text{If } \varepsilon_y < \varepsilon_s \le \varepsilon_{\text{sh}}, \text{ then } f_s = f_y \\
&\text{If } \varepsilon_s \ge \varepsilon_{sh}, \text{ then } f_s = f_y + (\varepsilon_s - \varepsilon_{sh}) * E_{sh} \\
&f_s' = \varepsilon_s' E_s
\end{aligned} \qquad (2\text{-}13)$$

$$f_p = \varepsilon_p E_p \qquad (2\text{-}14)$$

4) Calculate the resultant concrete compression force and location of the resultant concrete compression force, $\bar{x}$, measured from the neutral axis. Use the modified Hognestad model shown in Figure 2.3 for the concrete stress-strain relationship.

$$C_c = \int_0^c f_c b dy \qquad (2\text{-}15)$$

$$\bar{x} = \frac{\int_0^c f_c \text{bydy}}{\int_0^c f_c \text{bdy}} \qquad (2\text{-}16)$$

5) Compute the tension and compression forces in the longitudinal steel and composite.

$$\begin{aligned}
C_s &= A_s' f_s' \\
T_s &= A_s f_s \\
T_p &= A_p f_p
\end{aligned} \qquad (2\text{-}17)$$

6) Check equilibrium.

$$\text{Is } C_c + C_s = T_s + T_p? \qquad (2\text{-}18)$$

7) Repeat steps 2 through 6 until $T_s + T_p = C_s + C_c$.

8) Compute the resultant location for the tensile force from top of the section.

$$g_T = \frac{(T_s * d_s + T_p * d_p)}{T_s + T_p} \quad (2\text{-}19)$$

9) Compute the resultant location for the compression force from top of the section.

$$g_C = \frac{(C_s * d'_s + C_c * (c - \bar{x}))}{C_s + C_c} \quad (2\text{-}20)$$

10) Compute flexural capacity of the strengthened cross section.

$$M_{ult} = (T_s + T_p) * (g_T - g_C) \quad (2\text{-}21)$$

2.4.3 Calculation of Flexural Capacity for Composite-Controlled Failure

Distributions of strain and stress corresponding to composite-controlled failure conditions are shown in Figure 2.6. The following procedures may be used to determine the corresponding flexural capacity of the strengthened cross-section.

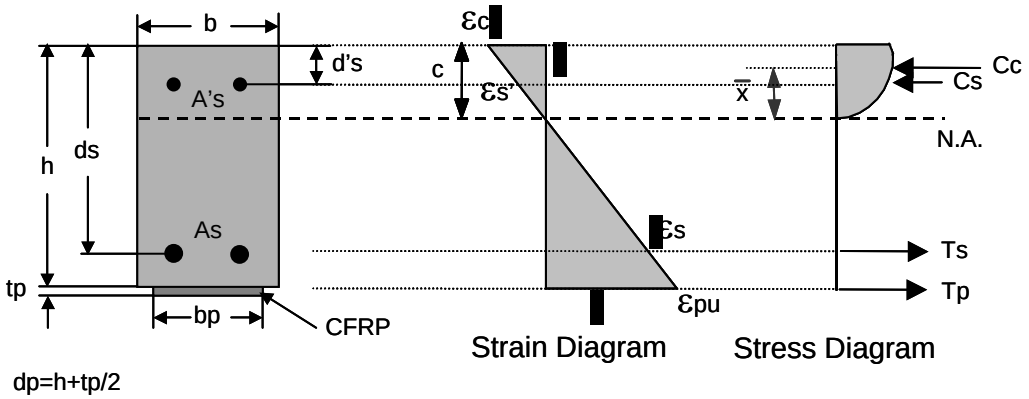

Figure 2.6: Stress and Strain Diagrams for Composite-Controlled Failure

1) $\varepsilon_p = \varepsilon_{pu}$

2) Assume c, then from strain compatibility compute ε_c, ε_s' and ε_s.

$$\varepsilon_c = \frac{\varepsilon_{pu} c}{(d_p - c)} \qquad (2\text{-}22)$$

$$\varepsilon_s = \frac{\varepsilon_{pu}(d_s - c)}{(d_p - c)} \qquad (2\text{-}23)$$

$$\varepsilon_s' = \frac{\varepsilon_c (c - d')}{c} \qquad (2\text{-}24)$$

3) Calculate steel stresses.

$$\begin{aligned} &\text{If } \varepsilon_s \le \varepsilon_y, \text{ then } f_s = \varepsilon_s E_s \\ &\text{If } \varepsilon_y < \varepsilon_s \le \varepsilon_{\text{sh}}, \text{ then } f_s = f_y \\ &\text{If } \varepsilon_s \ge \varepsilon_{sh}, \text{ then } f_s = f_y + (\varepsilon_s - \varepsilon_{sh}) * E_{sh} \\ &f_s' = \varepsilon_s' E_s \end{aligned} \qquad (2\text{-}25)$$

4) Calculate the resultant concrete compression force and location of the resultant concrete compression force, $\bar{x}$, measured from the neutral axis. Use the modified Hognestad model shown in Figure 2.3 for the concrete stress-strain relationship.

$$C_c = \int_0^c f_c b dy \qquad (2\text{-}26)$$

$$\bar{x} = \frac{\int_0^c f_c \text{by} d\text{y}}{\int_0^c f_c \text{b} d\text{y}} \qquad (2\text{-}27)$$

5) Compute the tension and compression forces in the longitudinal steel and composite.

$$\begin{aligned} C_s &= A_s' f_s' \\ T_s &= A_s f_s \\ T_p &= A_p f_{pu} \end{aligned} \qquad (2\text{-}28)$$

6) Check equilibrium.

$$\text{Is } C_c + C_s = T_s + T_p? \qquad (2\text{-}29)$$

7) Repeat steps 2 through 6 until $T_s + T_p = C_s + C_c$.

8) Compute the resultant location for tensile force from top of the section.

$$g_T = \frac{(T_s * d_s + T_p * d_p)}{T_s + T_p} \qquad (2\text{-}30)$$

9) Compute the resultant location for the compression force from top of the section.

$$g_C = \frac{(C_s * d'_s + C_c * (c - \bar{x}))}{C_s + C_c} \quad (2\text{-}31)$$

10) Compute flexural capacity of the strengthened cross section.

$$M_{ult} = (T_s + T_p) * (g_T - g_C) \quad (2\text{-}32)$$

Chapter 3: Experimental Program

3.1 INTRODUCTION

This chapter presents a detailed description of the experimental program. Twenty rectangular, reinforced concrete beams were fabricated in Ferguson Structural Engineering Laboratory. Eighteen of these beams were strengthened with carbon fiber composites to enhance flexural capacity before they were loaded to failure.

3.2 SPECIMEN DETAILS

3.2.1 Description of Beam Sections

Because of differences in strength of the carbon fiber composites selected for strengthening the rectangular reinforced concrete beams, two sizes of beams were used in the experimental program: 8"x14" by 9’-6” and 8”x16” by 10’-6”. Each beam was reinforced with two #5 bottom bars, two #3 top bars and No. 6 gage wire stirrups spaced 4 in. on center. See Figure 3.1 for the reinforcement details. In order to create a baseline for comparison of results, the first crack was forced to occur at a point of maximum moment, defined in section 3.2.2.1. This crack is referred to as the crack initiator and was created by placing a small piece of sheet metal, approximately 0.015 in. thick and extending 0.25 in. deep, across the full width of the beam. The maximum strains in the beam were measured at this location.

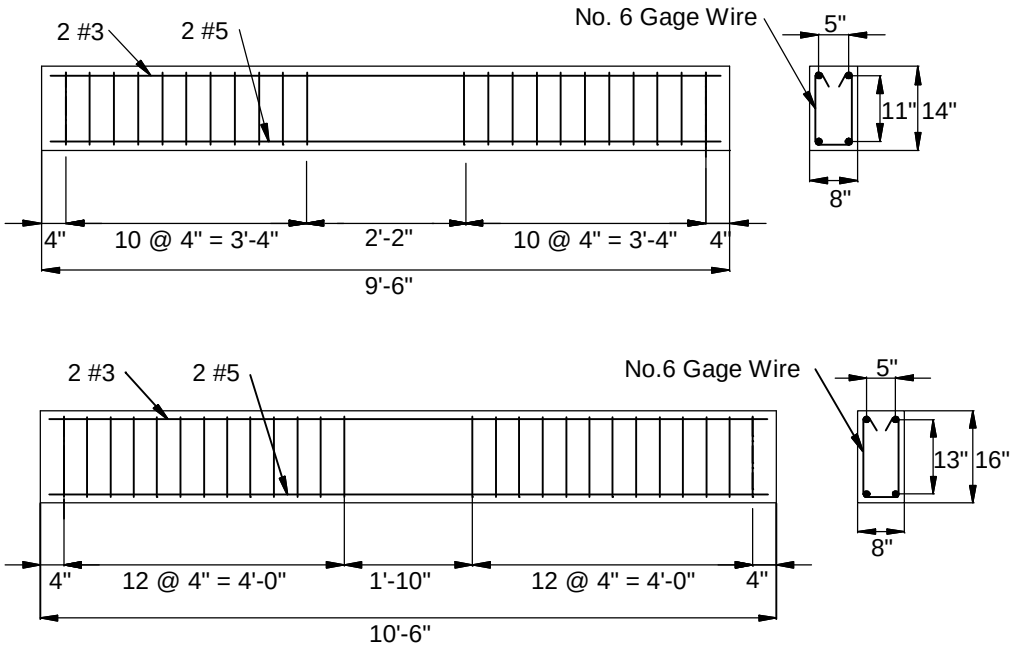

Figure 3.1: Details for the Reinforced Concrete Beams

3.2.2 Composite Strengthening Schemes

Because the primary objective of this portion of the research study was to identify effective methods for attaching carbon fiber composites to simply-supported reinforced concrete beams in order to increase their flexural strength, carbon fiber was first bonded to the bottom surface of the beams in order to use the material most efficiently. However, all of the early test specimens failed with the composites delaminated from the bottom surface of the concrete.

As testing progressed, it became apparent that bonding material to the sides, rather than the bottom of beams, might delay bond failure at the concrete/composite interface. Furthermore, the use of transverse composite straps was investigated for improving anchorage of longitudinal composite strips.

In all, four different configurations of the composites were investigated: bottom application, bottom application with transverse straps, side application, and side application with transverse straps (Figure 3.2 through 3.5). Each configuration is discussed in the following subsections.

3.2.2.1 Bottom Application

The experimental parameters in this phase of the study were selected to investigate the effect of bonded length of composite, relative to a critical section, on anchorage of the carbon fiber composite for flexural strengthening. Carbon fiber composite was bonded to the extreme tension fibers and is referred to herein as "bottom application". Composite material was bonded almost the full length of the shear span on one end of each beam. The other end had the composite bonded a specified distance from a crack initiator that was located beneath the closest load point. The distance from the crack initiator to the end of the composite was defined as the bonded length (Figure 3.2).

The objectives of the tests with the CFRP applied to the bottom surface of the cross section were to compare strengths obtained from beams with different bonded lengths and identify the bonded length necessary to develop the strength of the carbon fiber composite. The tests were intended to be analogous to tests conducted to define development length of reinforcing bars (Ferguson, 1962).

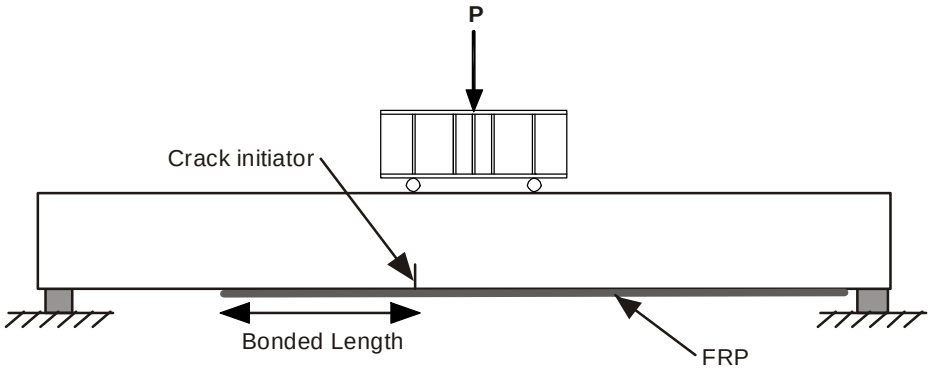

Figure 3.2: Schematic of Bottom Application

3.2.2.2 Bottom Application with Transverse Straps

Test specimens with bottom application of the composite tended to fail prematurely because vertical movement along cracks caused the composites to debond from the bottom surface of the cross section. Because specimens with bottom application of the composite did not develop the strength of the composite, even when the material was bonded over nearly the entire shear span, an enhancement was needed to prevent the composite from debonding prematurely.

Several publications have suggested using bolts to help anchor the composite to the concrete cross section (Spadea, 1998). This option was dismissed because the composite fibers, which are unidirectional, would likely split and pull out around the bolt. Other recommendations include clamping the composite with plates and bolts or clamping the composite with transverse composite straps.

The option chosen was transverse composite straps (Figure 3.3). The straps were similar to those tested previously to enhance shear strength (Triantafillou, 1998). Narrow, 2-in. wide composite strips were placed over the longitudinal composite and up the side faces of each beam 3 in. from the top surface of the beam. The straps, which were spaced at h/2 on center, were intended to permit some debonding between straps while keeping the composite anchored, and to restrain shear cracks in order to prevent vertical offsets from occurring along the bottom face of beams.

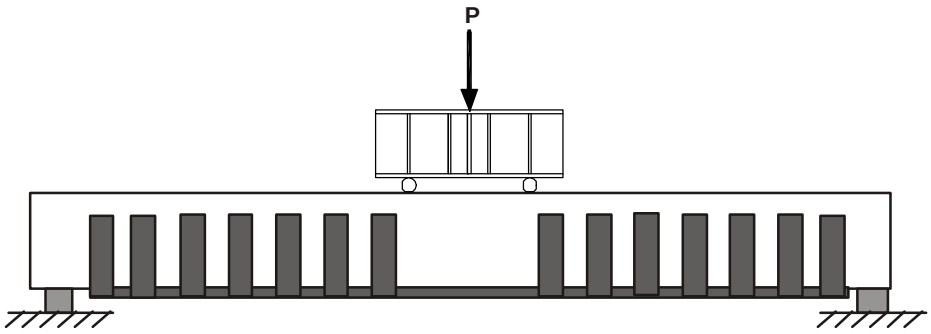

Figure 3.3: Schematic of Bottom Application with Transverse Straps

3.2.2.3 Side Application

Because bottom application of the composite (without transverse straps) tended to result in sudden debonding of the material due to a vertical offset at some crack locations on the bottom face of beams, side application of the composite (Figure 3.4) was tried to determine if this application would be less affected by the relative displacement at crack locations.

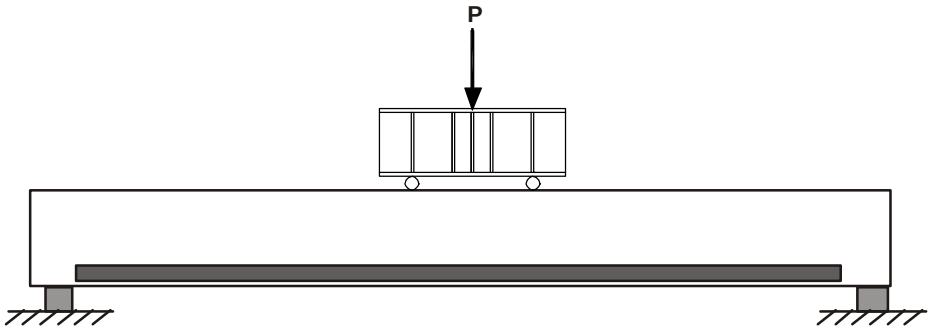

Figure 3.4: Schematic of Side Application

3.2.2.4 Side Application with Transverse Straps

Beams with composite material applied to side faces generally failed because of debonding at the composite/concrete interface and/or tensile failure of the concrete adjacent to the composite. Transverse straps, similar to those used with the bottom application, were attached to provide additional anchorage for the longitudinal carbon fibers and to distribute interface stresses to more concrete.

As for the bottom application case, straps were 2 inches wide and were spaced h/2 on center.

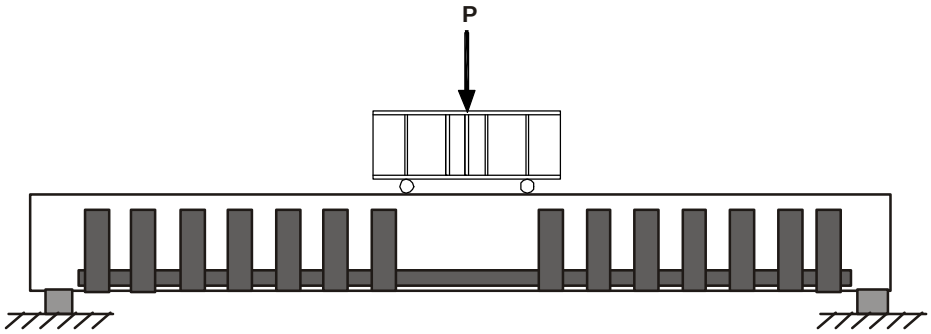

Figure 3.5: Schematic of Side Application with Transverse Straps

3.2.3 Overview of Test Program

A series of twenty specimens was tested. Two of the specimens were unstrengthened to provide baseline strength and deformation data to be used in evaluating the response of strengthened specimens. Test variables included application type and method, composite type and manufacturer, number of plies of composite material applied, bonded composite length, number of transverse straps applied, and effect of surface preparation. Table 3.1 summarizes the test program.

Table 3.1: Summary of Test Program

Specimen	Concrete Batch #	Composite Type	# of Plies	Approximate Width of Plies	Bonded Length (in)	# of Transverse Straps Along Shear Span	Application Type	Concrete Surface Preparation
Control A&B	I	-	-	-	-	-	-	-
A1	I	A	2	2"	10	0	Bottom	Grind
A2	I	A	2	2"	14	0	Bottom	Grind
A3	I	A	2	2"	30	0	Bottom	Grind
A4	II	A	1	4"	15	0	Bottom	Grind
B1	II	B	2	3"	35	0	Bottom	Grind
B2	II	B	2	2"	35	7	Bottom w/ Straps	Grind
B3	II	B	2	2"	35	0	Side	Grind
B4	III	B	2	2"	35	4	Bottom w/ Straps	Grind
B5	III	B	2	2"	24	4	Bottom w/ Straps	Grind
Control C&D	I	-	-	-	-	-	-	-
C1	I	C	2	2"	45	0	Bottom	Grind
C2	I	C	2	2"	45	0	Bottom	Sand-blast
C3	I	C	2	2"	45	7	Bottom w/ Straps	Grind
C4	I	C	2	2"	45	0	Side	Grind
D1	II	D	1	2"	45	0	Bottom	Grind
D2	II	D	1	2"	45	0	Bottom	Sand-blast
D3	II	D	2	2"	45	0	Side	Grind
D4	III	D	2	2"	45	7	Side w/ Straps	Grind
D5	III	D	2	2"	30	4	Side w/ Straps	Grind
Note: Specimens strengthened with A and B composite were 8" x 14" x 9'-6".								
Specimens strengthened with C and D composite were 8" x 16" x 10'-6".								
Specimens from concrete batch I and II used steel from Heat 1.								
Specimens from concrete batch III used steel from Heat 2.								

3.3 TEST SETUP

The test setup was designed to apply a two-point loading to beams strengthened with carbon fiber composites. Load was applied using a 140-kip capacity Enerpac hydraulic ram in conjunction with a stiffened steel wide flange section placed on nested rollers on top of the beam (Figures 3.6 and 3.7). Beams were supported by 3”x7”x2” neoprene bearing pads that were placed on concrete pedestals capable of accommodating both the 9’-6” and 10’-6” spans.

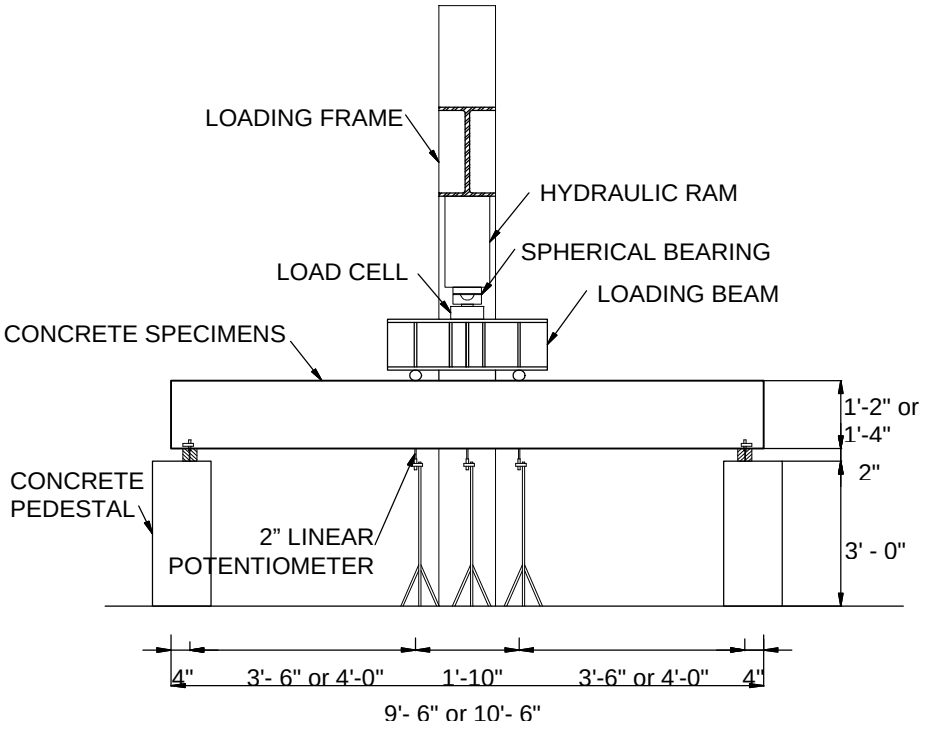

Figure 3.6: Elevation of Test Setup

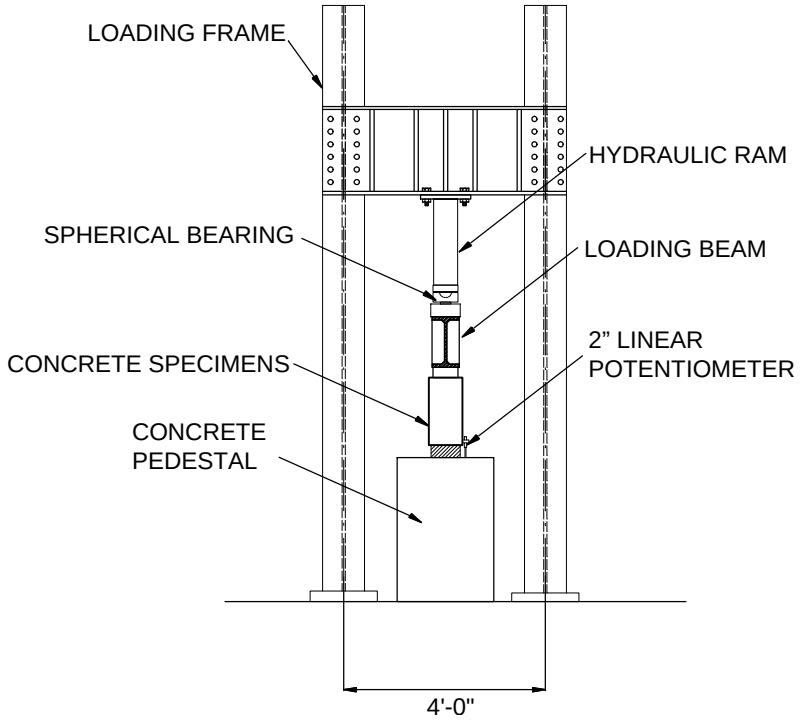

Figure 3.7: End View of Test Setup

3.4 LOADING PROGRAM

Each beam was tested by applying monotonically-increasing loads to failure. Load was applied at two points spaced 22 in. apart and centered along the span in approximately 1500-lb increments (3000-lbs total) until yield. Beyond yield, midspan displacement of beams was increased in approximately 0.15-in. increments until failure occurred. Between load or displacement increments, beams were inspected for cracks and for damage to the composite strengthening system. Crack patterns were recorded, critical crack widths were measured, and damage was photographed. Because of leakage in the hydraulic system, loads on

beams dropped during the inspection process. This load was reapplied before proceeding to the next load or displacement increment.

3.5 MATERIAL PROPERTIES

3.5.1 Concrete

A total of twenty specimens were constructed using three batches of concrete. The strength-age curve for each batch of concrete is shown in Figure 3.8. For each batch, cylinders were typically tested after 3, 7, 14, and 28 days at a rate of 50 kips/minute to measure the concrete compressive strength (Tables 3.2, 3.3, and 3.4). Instead of testing cylinders the day of every beam test, cylinders were tested the first day of beam testing (second to last entry in Tables 3.2, 3.3, and 3.4) and the last day of beam testing (the last entry in Tables 3.2, 3.3, and 3.4) for each concrete batch. These strengths typically correspond to different ages depending on the batch because of the flexible testing schedule. These average cylinder strengths on the first and last day of beam testing were used to calculate the average cylinder strength for each batch of concrete. Because cylinder strengths did not vary significantly, an average of the test day strengths was computed (Table 3.5) and used for f_c' in the calculation of specimen capacities.

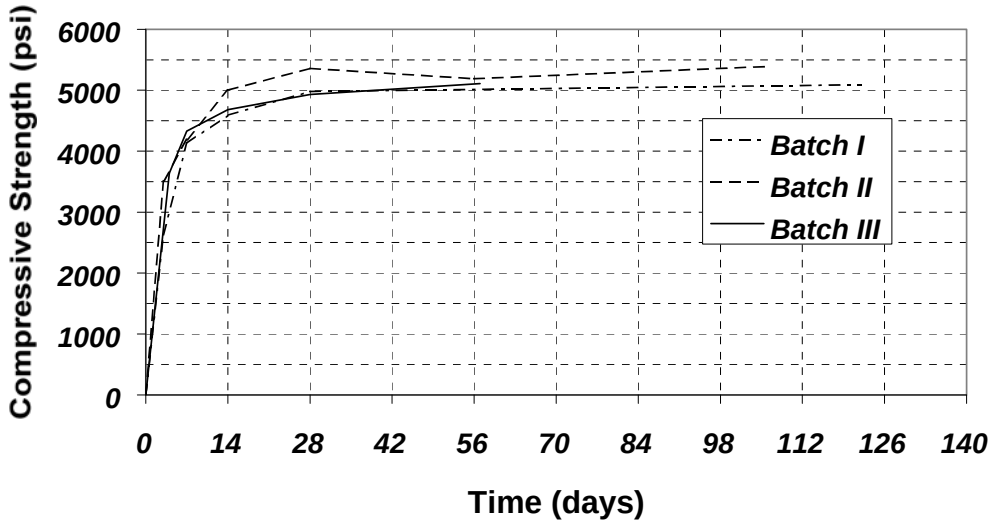

Figure 3.8: Strength - Age Curve

Table 3.2: Cylinder Data for Concrete Batch I

No. Days	No. of Cylinders	Average f'c (psi)	Standard Deviation (psi)
3	2	2630	260
7	3	4130	40
14	2	4590	160
28	3	4980	50
122	2	5090	110

Table 3.3: Cylinder Data for Concrete Batch II

No. Days	No. of Cylinders	Average f'c (psi)	Standard Deviation (psi)
3	3	3510	120
7	3	4190	100
14	3	5000	110
28	2	5360	160
56	2	5190	130
106	2	5390	320

Table 3.4: Cylinder Data for Concrete Batch III

No. Days	No. of Cylinders	Average f'c (psi)	Standard Deviation (psi)
4	3	3640	120
7	3	4330	120
14	3	4680	380
28	3	4930	50
57	2	5110	290

Table 3.5: Average Concrete Compressive Strength on Day of Test

Batch #	Average f'c (psi)
I	5040
II	5290
III	5020
Average	5120

Two cylinders were tested from Concrete Batch III to obtain a representative stress-strain relationship for the concrete. The value for ε_0 was

taken from these curves as 0.0016 and ε_{cu} was chosen as 0.0035 for use in the modified Hognestad model (Hognestad, 1951) during the calculation of specimen capacities. The curves are shown in Figure 3.9.

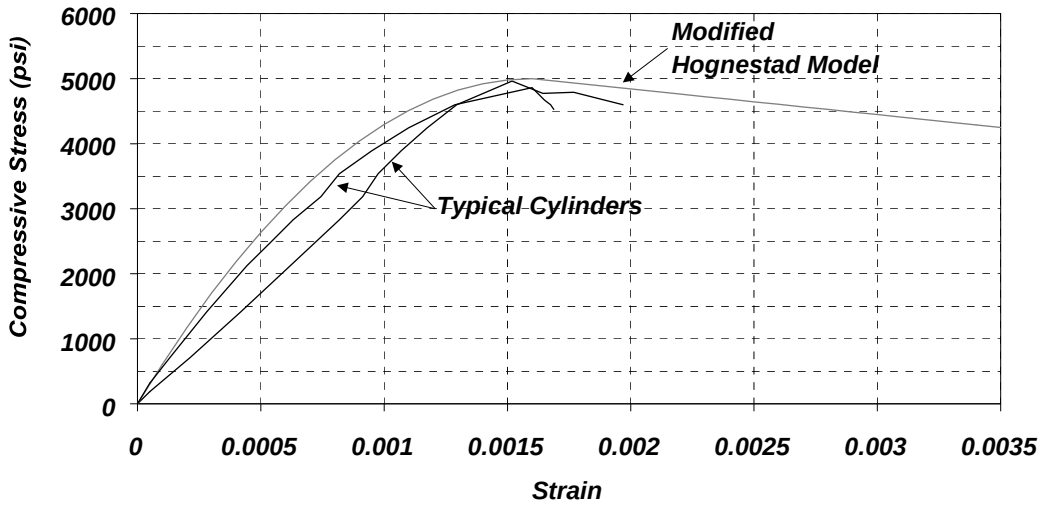

Figure 3.9: Stress-Strain Relationship for Concrete in Compression

3.5.2 Steel Reinforcement

Reinforcement had a nominal yield stress of 60 ksi. To determine the actual stress-strain relationship for the steel reinforcement, tension coupons were tested at a maximum strain rate of 0.0025/minute. Two #5 bars were tested from the first batch of steel that was received, Heat 1, and three were tested from Heat 2. For beam capacity calculations, an idealized tri-linear relationship was used to represent the stress-strain response for the steel reinforcement. The model developed for each heat of steel is shown in Figures 3.10 and 3.11 along with the measured stress-strain response for the bars tested.

The yield stress of compression reinforcement, #3 bars, was determined from testing to be 60 ksi for Heat 1 and 66 ksi for Heat 2. Unlike the tensile reinforcement, the compression reinforcement did not yield during testing. Therefore, the complete stress-strain relationship was not measured for the #3 bars.

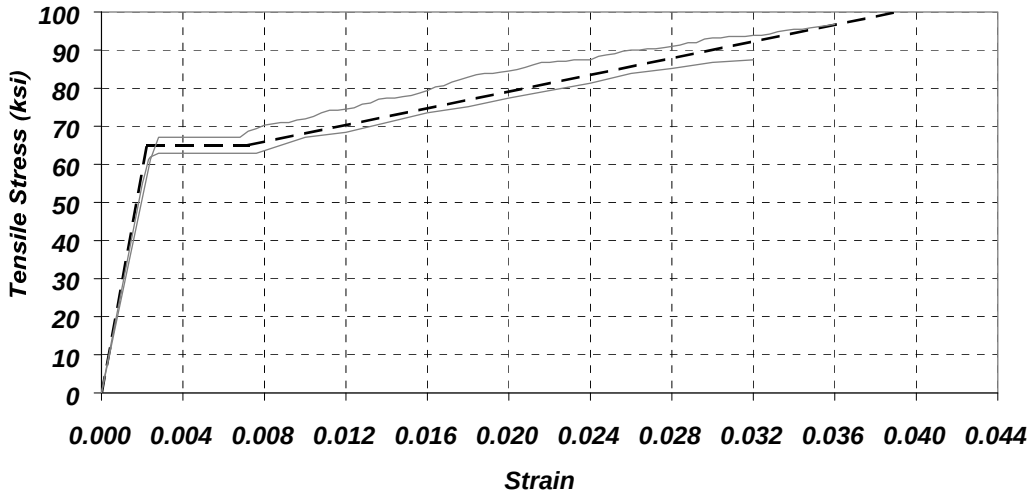

Figure 3.10: Stress Strain Response for No. 5 Bars from Heat 1

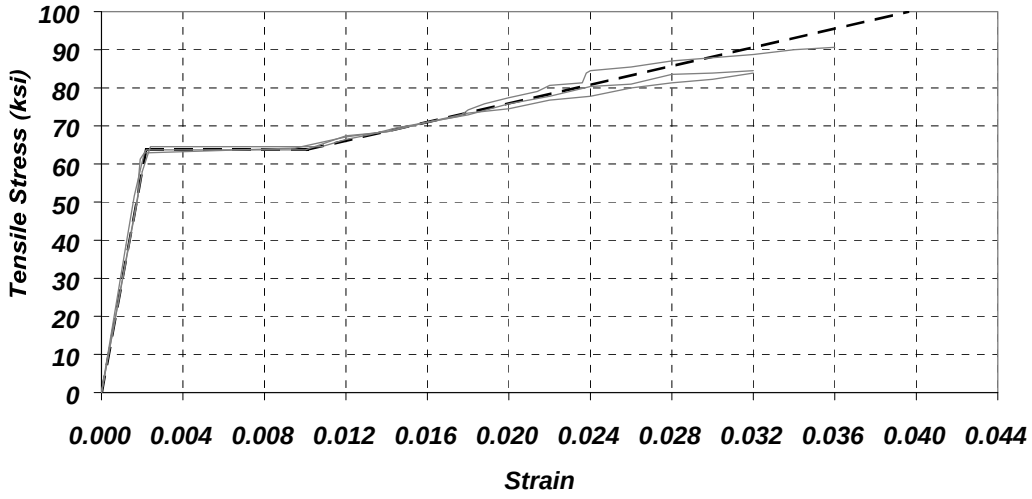

Figure 3.11: Stress Strain Response for No. 5 Bars from Heat 2

3.5.3 Composite Material

3.5.3.1 Types & Application Method

Composite fiber systems are available in many forms. Fibers can be made of glass, aramid, carbon, or graphite. Unidirectional, carbon fibers were chosen for testing because of the higher modulus and tensile strength associated with the material. As a result, less material was needed compared with other composite materials to obtain the same capacity for the strengthened beams. Carbon fiber also is lightweight and has excellent fatigue resistance compared with other composites (Inoue, 1995). Carbon fiber composites also have better long-term performance because they are not susceptible to creep, which can control the behavior of glass composites. These fibers can be manufactured and applied in several ways.

Carbon fiber composites are made of two materials: resin and carbon fibers (Figure 3.12). The resin provides for transfer of force between individual fibers. It also provides some compressive strength and chemical protection. The fibers provide stiffness and tensile strength to the system.

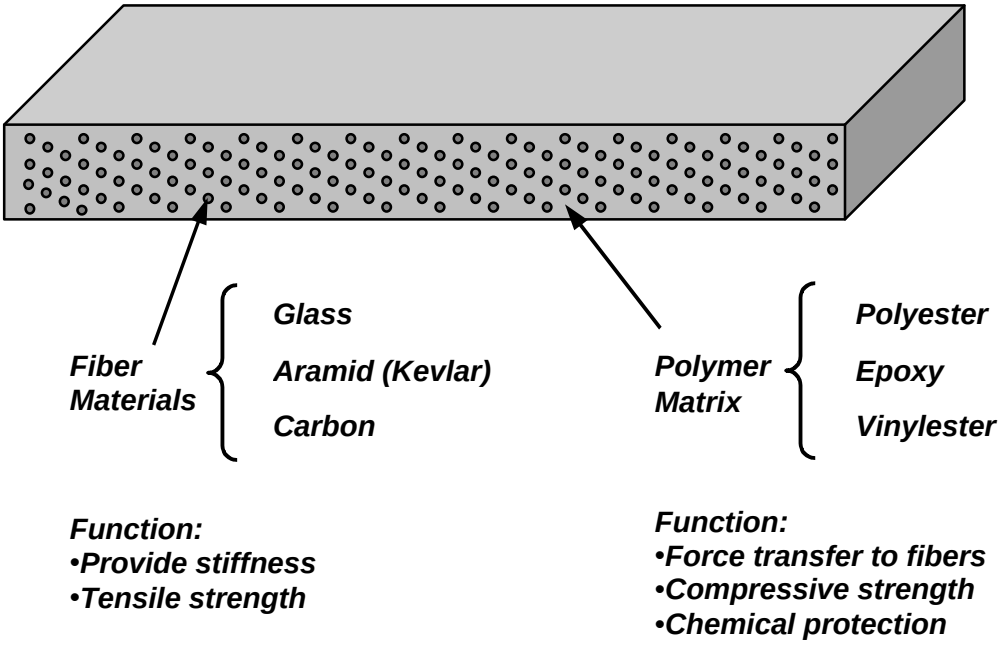

Figure 3.12: Composite Matrix

a) Wet Lay-up

One type of composite application is the wet lay-up system illustrated in Figure 3.13. This system arrives on site as a roll of flexible, unidirectional fibers and several containers of epoxy components. These flexible sheets can conform to nearly any concrete surface. Epoxy for this system is very fluid and is intended to act not only as the bonding agent but also form the composite matrix. Fabric

fibers are produced in several forms as shown in Figures 3.14 and 3.15. Two forms were used for these tests: a tow sheet and a weave. The tow sheet is a layer of unidirectional fibers attached to a sheet of paper. The paper is used only for application purposes. The fabric weave is bundles of unidirectional fibers woven with transverse fibers. The transverse fibers are a small fraction of the longitudinal fibers and are intended only to maintain integrity of the main fibers during application.

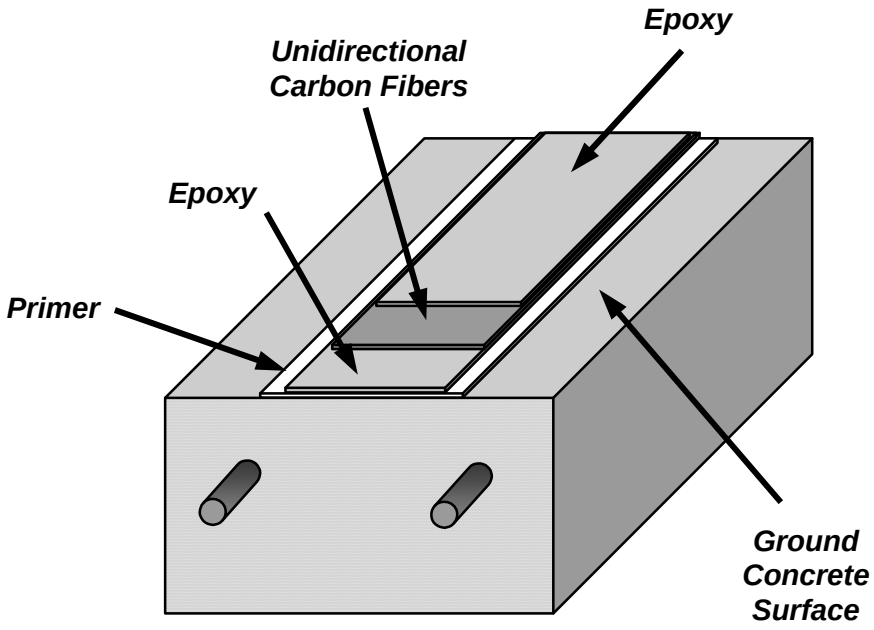

Figure 3.13: Schematic of Wet Lay-up Composite Application Components

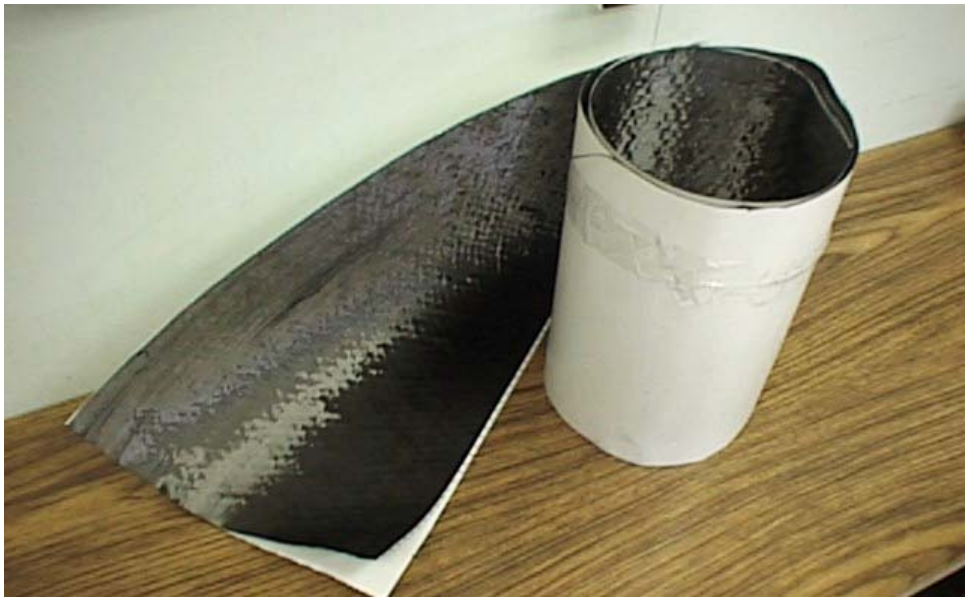

Figure 3.14: Tow Sheet Flexible Fiber Type

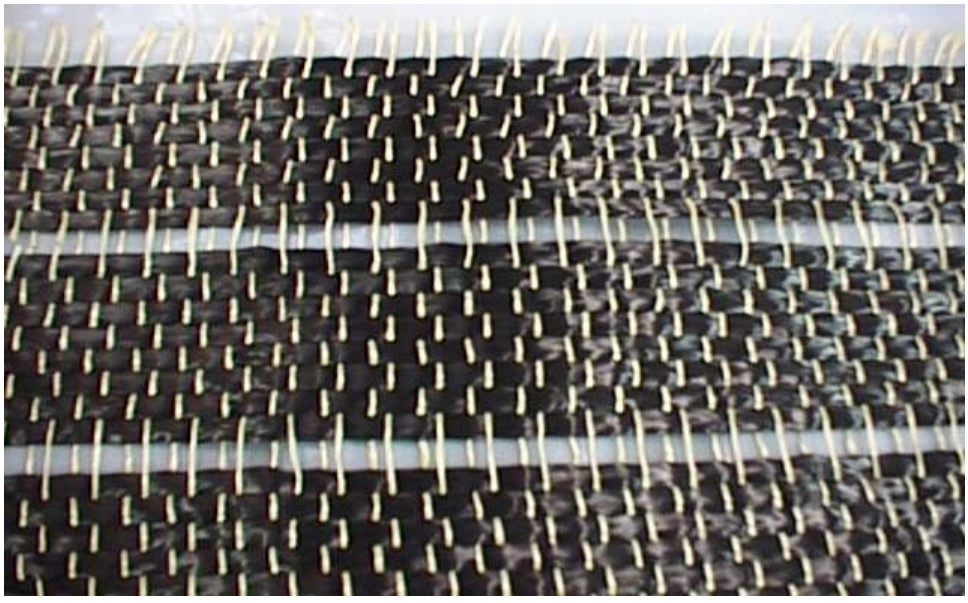

Figure 3.15: Fabric Weave Flexible Fiber Type

The application process begins by preparing the concrete surface. It is important to grind the concrete surface to smooth any irregularities, remove scale, and roughen the surface to enhance bond between the fiber composite and concrete (Figure 3.16). Once the surface has been properly ground, all dust must be removed from the surface by cleaning with a cotton towel and acetone to achieve good bond. After the surface is prepared, it is recommended by the manufacturers to use an epoxy primer to seal the concrete surface (Figure 3.17). Epoxies used in the wet lay-up system have low viscosity and are easily absorbed by the concrete. The primer is applied first to ensure the concrete does not absorb the epoxy needed to impregnate the composite material and form the composite matrix.

Figure 3.16: Surface Preparation

Figure 3.17: Application of Primer

The next step in the process is cutting the fabric to the desired size (Figure 3.18). Then the epoxy is mixed according to manufacturer specifications and applied to the prepared surface of the concrete. At this point, the process varies from product to product. The objective of the next step, which can be done in several ways, is to impregnate the fibers with epoxy to form the composite matrix. Two different methods are described below.

Figure 3.18: Fiber Preparation

Method 1 begins by applying the epoxy to the surface of the concrete and then applying the fibers over this layer of epoxy (Figures 3.19 and 3.20). Once the fibers are in place, it is recommended by the manufacturer to wait approximately 20 minutes to allow the epoxy to impregnate the fibers before applying the final coat of epoxy. Finally, the composite is allowed to cure at room temperature for seven days.

Figure 3.19: Wet Lay-up Method 1 Epoxy Application

Figure 3.20: Wet Lay-up Method 1 Fiber Application

Method 2 begins by applying the epoxy to the prepared surface of the beam (the particular application shown in Figure 3.21 does not have a primer applied to the surface). Then the fibers must be immersed in epoxy (Figure 3.22) before applying the fibers to the concrete surface (Figure 3.23). Then a final coat of epoxy is applied to the fibers once they are in place. Finally, the composite is allowed to cure at room temperature for seven days.

Figure 3.21: Wet Lay-up Method 2 Epoxy Application

Figure 3.22: Wet Lay-up Method 2 Fiber Saturation

Figure 3.23: Wet Lay-up Method 2 Fiber Application

Variability in composite behavior is introduced because of the many steps required in the wet lay-up process. It is important to follow manufacturer procedures carefully in order to control the quality of the composite matrix.

b) Pultruded

Another type of composite system is the pultruded system illustrated in Figure 3.24. This system arrives on site in the form of stiff, thin plates that can be applied only to flat surfaces. The plates are quite stiff because the fibers have been pre-impregnated in a fluid epoxy at the manufacturing plant.

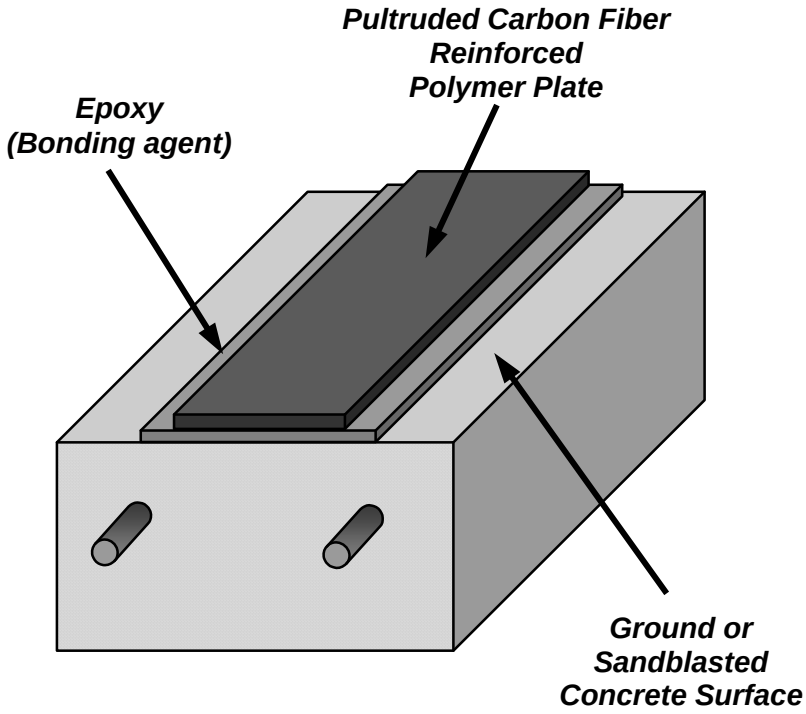

Figure 3.24: Schematic of Pultruded Composite Application Components

The pultrusion process begins with a roving of fiber bundles that are pulled through an epoxy or resin bath. The epoxy bath impregnates the fibers to form the composite. The impregnated fibers are then pulled through a pre-former where they are given a general cross-section shape. Then they are pulled through the forming and curing die where the composite is given its final shape and is cured. Finally, the composite is cut to the desired length requested by the purchaser. The process is summarized in Figure 3.25.

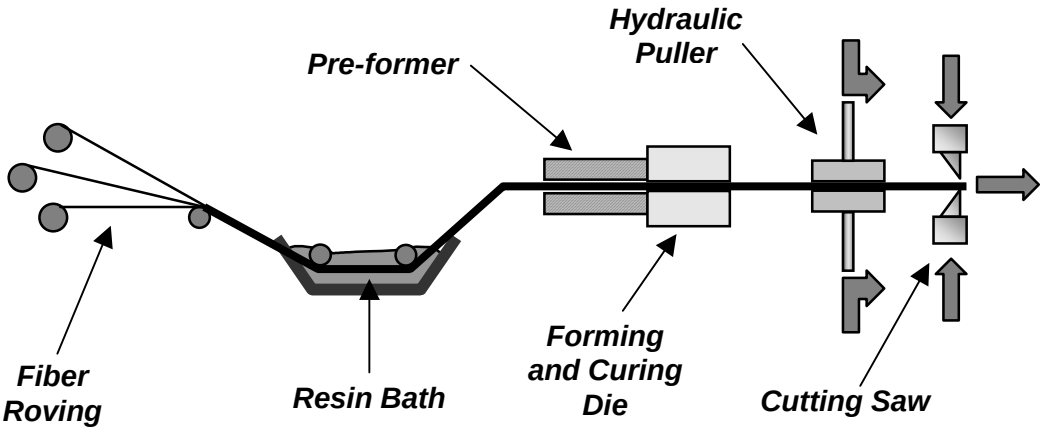

Figure 3.25: Pultrusion Process

The pultruded application process begins with surface preparation by grinding or sandblasting the surface. With pultruded systems, no primer is needed. There is no fear of the concrete absorbing epoxy needed to form the composite matrix because the fibers have been pre-impregnated at the manufacturing plant. The next step in the process is cleaning the composite with a clean towel and acetone (Figure 3.26). Then a thin layer of epoxy (1/16" to 1/8") is applied to the composite surface and concrete surface (Figures 3.27 and 3.28). If the epoxy is too thick, bond will likely be compromised because the epoxy will be required to resist force for which it was not designed. The epoxy for this system is viscous and acts only as a bonding agent between the fiber composite and concrete surface. Next, the plates are pressed into place against the epoxy and a roller is used to press all excess epoxy and air pockets out from under the plate (Figures 3.29 and 3.30). Excess epoxy is removed and the system is allowed to cure for seven days.

Figure 3.26: Cleaning Composite

Figure 3.27: Epoxy Application to Composite

Figure 3.28: Epoxy Application to Concrete Surface

Figure 3.29: Composite Application

Figure 3.30: Rolling Composite to Remove Excess Epoxy and Air Voids

Pultruded composites offer better quality control in the formation of the composite matrix because they are fabricated in a controlled environment. However, uses for the material are limited because the system is quite stiff and cannot conform to all surfaces.

3.5.3.2 Material Properties

Five different carbon fiber composite systems were used in this study. Material properties varied from product to product even though the main ingredient in the composite was carbon fibers. Each manufacturer has its own standards for producing and testing their product. Material properties are tabulated in Table 3.6. Composite thickness is the design thickness and is defined as the carbon fiber thickness for use in calculating force in the composite for one ply of material. The manufacturer publishes this value. Composite strength is the tensile strength of the composite matrix. The composite modulus is the modulus of elasticity for the composite matrix and is defined as the slope of the stress-strain response for the material. This property is also provided by the manufacturer. The products listed in Table 3.6 were provided by Fyfe, Master Builders, Mitsubishi/Replark, and Sika, and the product properties were obtained from the respective product specifications.

Table 3.6: Carbon Fiber Composite Material Properties as Published by Manufacturers

	A	B	C	D	E
Composite Thickness (in)	0.0065	0.0066	0.041	0.047	0.040
Composite Strength (ksi)	505	493	110	348	139
Composite Modulus (ksi)	33,000	33,400	9,000	22,500	10,600
Elongation at Failure (%)	1.5	1.5	1.2	1.9*	1.33
Composite Type	Wet Lay-up	Wet Lay-up	Wet Lay-up	Pultruded	Wet Lay-up
Manufacturer	Master Builders	Mitsubishi	Fyfe	Sika	Sika

*Strain as published by manufacturer. $f_{pu}/E_p=1.55$

3.6 INSTRUMENTATION AND DATA ACQUISITION

Strain gages were bonded to steel reinforcing bars, side faces of the beam in the concrete compression zone, and on carbon fiber composites typically at the critical section (Figure 3.31). The crack initiator was located directly under one load point and was used to define the critical section, which also defined the edge of the constant moment region of the beam. A section was also instrumented at a location halfway between the critical section and the end of the composite in specimens from batch II and III. The concrete gages, CG1 and CG2, had a 60-mm gage length. The steel gages, SG1, SG2, and SG3, and the CFRP gage, CFRP1, had either a 5-mm or 6-mm gage length depending on availability of gages.

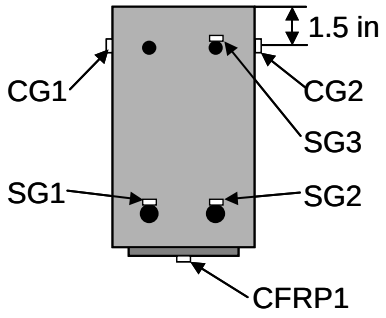

Figure 3.31: Strain Gage Locations

Five 2-in. linear displacement potentiometers were used to measure displacements at or near midspan and at the supports (Figure 3.6). Displacement potentiometers at the support locations on opposite sides of the beam were used to measure compression of the bearing pads and to check for possible torsional effects from misalignment of the loading ram.

Total applied load was measured with a 50-kip capacity Strainsense load cell placed between the spherical bearing and the steel wide-flange spreader beam used to apply load at two points on the beam.

Electronic readings from the instruments were collected every 2 seconds during loading using a Hewlett Packard 75000 scanner and were stored in spreadsheet format on a personal computer.

Chapter 4: Presentation and Evaluation of Test Results

4.1 OBJECTIVE

This chapter presents the results of monotonic load tests of twenty beam specimens, and evaluates the effectiveness of various carbon-fiber composite application schemes for flexural strengthening of reinforced concrete beams. Details of the testing program were presented in Chapter 3. General observations for the entire group of specimens are presented first, then specimen behavior is examined in four groups associated with the placement of the composites: bottom application, bottom application with transverse straps, side application, and side application with transverse straps.

4.2 QUANTITIES CONSIDERED IN EVALUATION OF SPECIMEN BEHAVIOR

Yield load and displacement, ultimate load and displacement, displacement ductility, maximum measured strain, and computed capacity are summarized in Table 4.1 for all specimens.

Yield load and the corresponding deflection were taken as the point on the load-deflection response curve when stiffness of the beam changed dramatically (See Figure 4.1). Yield load was not identified from strain measurements, because measured strains corresponding with yield strain at the critical section tended to lag behind yielding at other locations between the points of load application.

Ultimate load and deflection (Figure 4.1) were easier to identify for the specimens because the maximum load occurred when the composite material debonded, the composite ruptured, or concrete crushed.

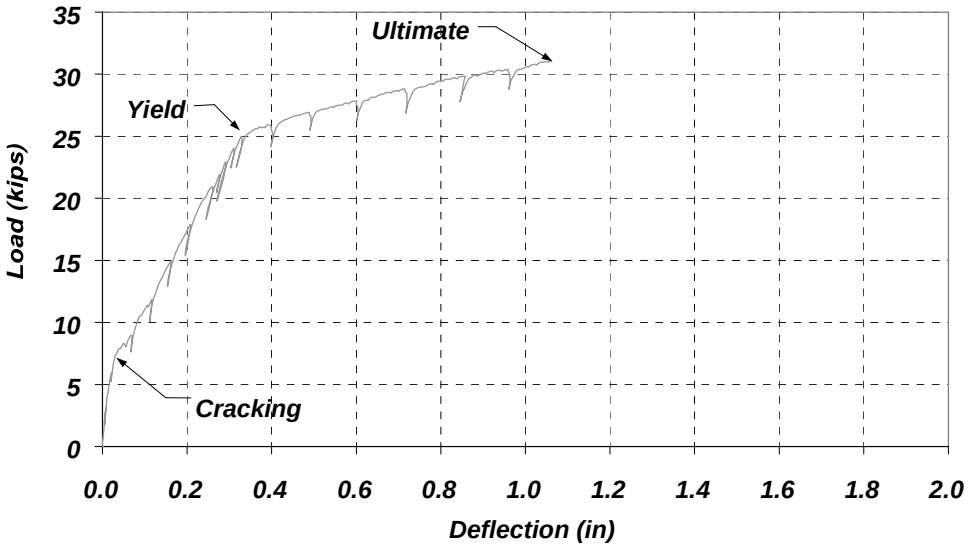

Figure 4.1: Typical Load-Deflection Response

One quantity used to compare the effectiveness of the carbon fiber strengthening scheme was the ratio of measured to computed capacity. The computed flexural capacity was determined using the procedure outlined in Chapter 2. The load corresponding to the computed flexural capacity was calculated using the specimen details described in Chapter 3 and statics.

Displacement ductility ratio was also used to compare specimen responses because ductility ratio is a relative indicator of specimen deformation capacity. The displacement ductility ratio was calculated as the ultimate deflection divided by the yield deflection.

CFRP strains were measured at the critical section in order to compare maximum measured strains with ultimate strain values published by the various composite manufacturers. To better compare the maximum measured strains from all specimens, measured strains were normalized with respect to the appropriate value of published ultimate strain. This ratio of measured strain to nominal strain capacity will hereafter be referred to as the strain ratio.

Table 4.1: Summary of Results for All Specimens

	Application Scheme	*Failure*	*Measured*				*Computed Capacity (kips)*	*% of Computed Capacity Achieved*	*Ductility Ratio* $\mu=\Delta_u/\Delta_y$	*Maximum Measured CFRP Strain*	*Published CFRP Strain*	*Strain Ratio*
			Yield Deflection (in)	*Yield Load (kips)*	*Maximum Deflection (in)*	*Maximum Load (kips)*						
Control A & B	None	Crushing	0.29	22.6	1.74	29.6	28.3	105%	6.0			
A1	Bottom	Debonding	0.31	23.9	0.45	26.9	31.3	86%	1.4	0.0079	0.0150	0.53
A2	Bottom	Debonding	0.32	24.1	0.59	28.3	31.3	90%	1.9	0.0061	0.0150	0.41
A3	Bottom	Debonding	0.32	24.3	1.06	31.1	31.3	99%	3.3	0.0120	0.0150	0.80
A4	Bottom	Debonding	0.31	24.8	0.75	29.0	31.3	93%	2.5	0.0078	0.0150	0.52
B1	Bottom	Debonding	0.34	25.1	0.76	29.9	33.8	89%	2.2	0.0072	0.0150	0.48
B2	Bottom w/ Straps	Fiber Rupture	0.34	24.9	1.12	31.9	31.3	102%	3.3	0.0113	0.0150	0.75
B3	Side	Fiber Rupture	0.34	24.5	1.13	30.8	30.7	100%	3.3	0.0107	0.0150	0.71
B4	Bottom w/ Straps	Fiber Rupture	0.31	23.8	1.07	29.8	30.5	98%	3.4	0.0119	0.0150	0.79
B5	Bottom w/ Straps	Fiber Rupture	0.31	24.7	0.91	29.2	30.5	96%	2.9	0.0132	0.0150	0.88
Control C & D	None	Crushing	0.31	22.1	2.28	28.4	28.6	99%	7.3			
C1	Bottom	Debonding	0.34	25.4	0.90	32.3	34.1	95%	2.7	0.0076	0.0120	0.63
C2	Bottom	Debonding	0.34	24.8	0.65	28.8	34.1	84%	1.9	0.0070	0.0120	0.58
C3	Bottom w/ Straps	Fiber Rupture	0.33	26.5	0.98	33.7	34.1	99%	2.9	0.0075	0.0120	0.63
C4	Side	Debonding	0.32	26.0	0.92	30.0	33.6	89%	2.8	Unavailable	0.0120	
D1	Bottom	Debonding	0.32	26.9	0.42	28.9	40.1	72%	1.3	0.0035	0.0190	0.19
D2	Bottom	Debonding	0.33	27.2	0.54	30.3	40.1	75%	1.6	0.0048	0.0190	0.25
D3	Side	Debonding	0.34	29.9	0.62	36.0	46.6	77%	1.8	0.0044	0.0190	0.23
D4	Side w/ Straps	Debonding	0.34	30.4	0.91	42.3	45.8	92%	2.6	0.0065	0.0190	0.34
D5	Side w/ Straps	Debonding	0.35	29.8	0.84	40.7	45.8	89%	2.4	0.0062	0.0190	0.33

4.3 GENERAL OBSERVATIONS

Comments about the failure mode, percent of computed load achieved, and strain ratio are discussed for all strengthened specimens.

4.3.1 Observed Failure Modes

Only two of the three types of failure controlled the ultimate response of the specimens: debonding of the composite and rupture of the composite. Concrete crushing did not occur as expected in some specimens because The composite materials debonded prematurely. All specimens behaved similarly before yield. Each specimen exhibited an initial stiffness prior to cracking that was consistent with gross-section properties. Following cracking, stiffness was reduced by 8 to 28 percent. There was little evidence of distress in the composite before yield unless the bond length was extremely short.

After yield, epoxy in the wet lay-up system showed initial signs of distress through cracking and whitening in the vicinity of cracks, indicative of the early signs of local debonding of the CFRP (Figure 4.2). As load progressed, cracks in the epoxy adjacent to the composite material fanned out toward the composite as shown in Figure 4.3. The first evidence of debonding of the composite material occurred when these fan-shaped cracks turned parallel to the edge of the composite (Figure 4.4). As load was increased in specimens with no transverse straps, ultimate load was achieved by composite debonding (Figure 4.5). The debonding failure was sudden, and beams that experienced this type of failure exhibited limited ductility.

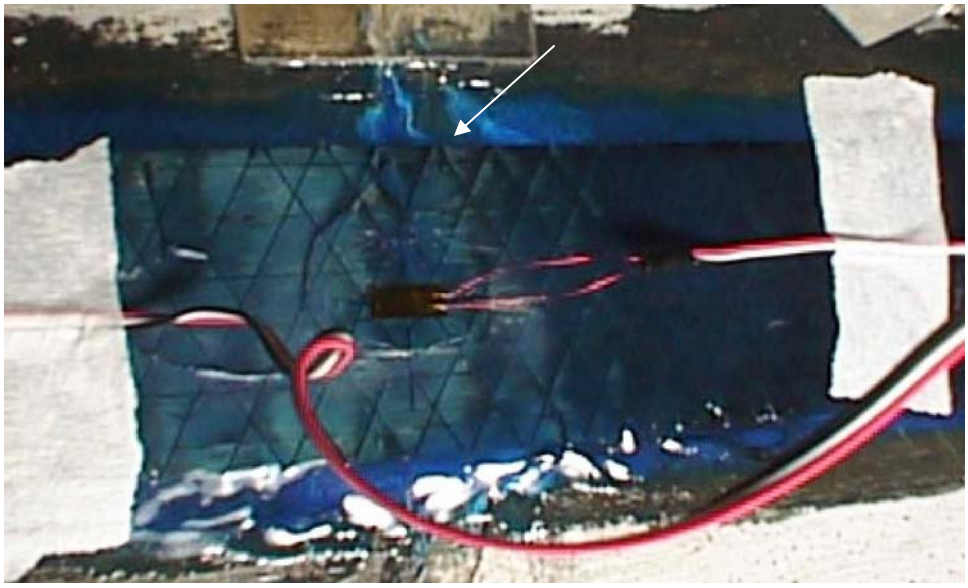

Figure 4.2: Initial Cracking in Epoxy

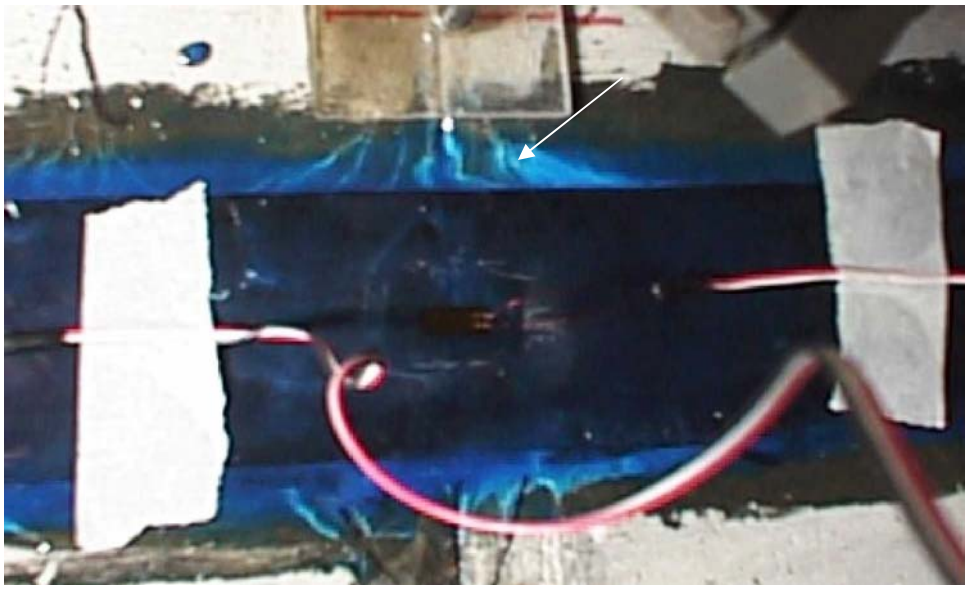

Figure 4.3: Whitening and Fanning of Cracks

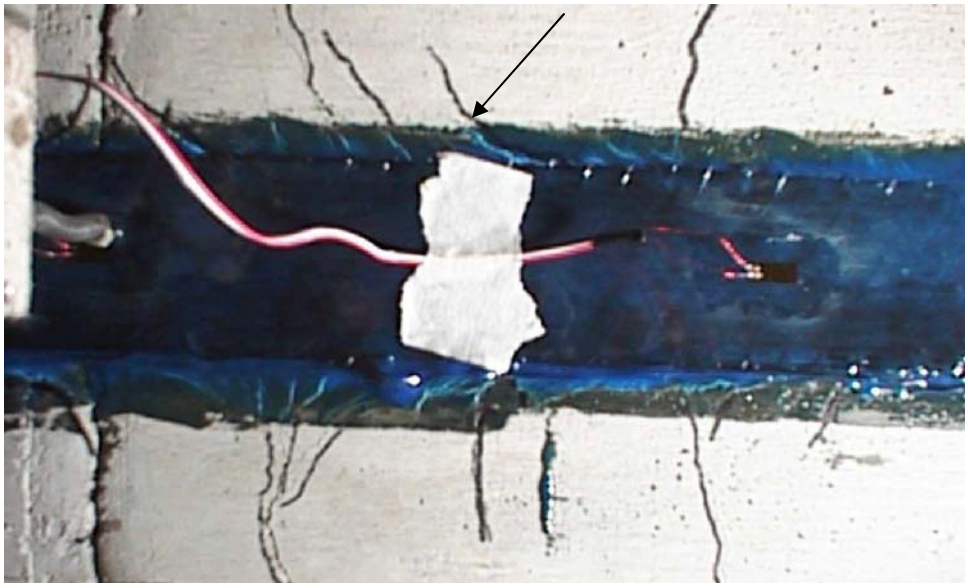

Figure 4.4: Initial Evidence of Debonding - Cracks Propagating Parallel to Composite

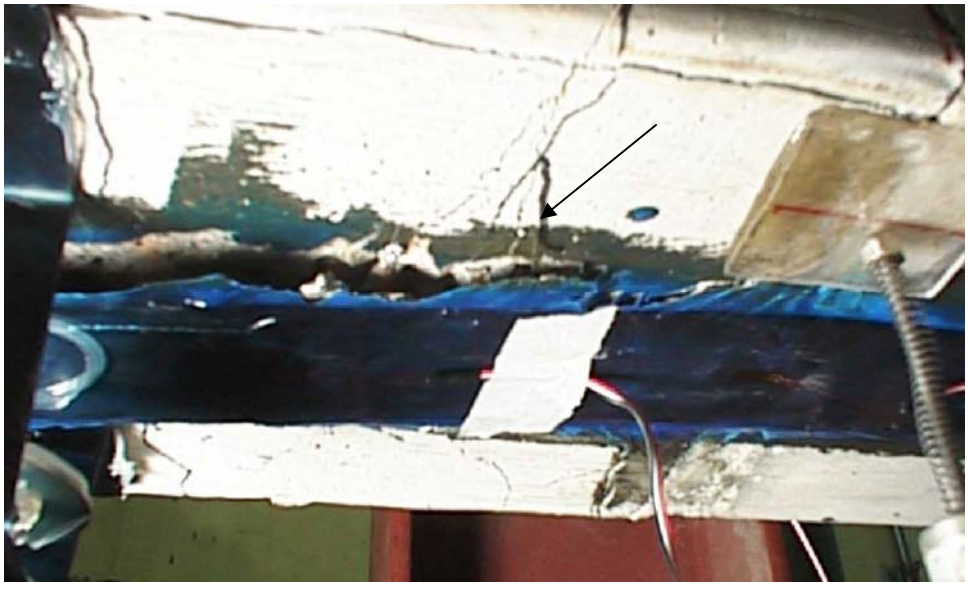

Figure 4.5: Debonding Failure

As alluded to previously, the initiation of debonding failure occurred at discrete crack locations. An example of a typical crack pattern for a beam on the verge of debonding failure is shown in Figure 4.6. Additional crack patterns at ultimate for other specimens are provided in Appendix A. As cracks developed along the shear span, a small, vertical, differential displacement occurred across the critical crack (Figure 4.7). This relative displacement of 1/16 to 1/8 in. worked to pry the composite from the bottom surface (Figure 4.8). Design equations for computing the required bonded length of composite fibers to be attached to concrete are based on average shear stresses between the concrete surface and composite. An offset at a flexure-shear crack results in tensile stresses between the composite and concrete on one side of the crack (Figure 4.9). Design equations published by the composite material manufacturers do not consider tensile stresses resulting from this prying action at crack locations.

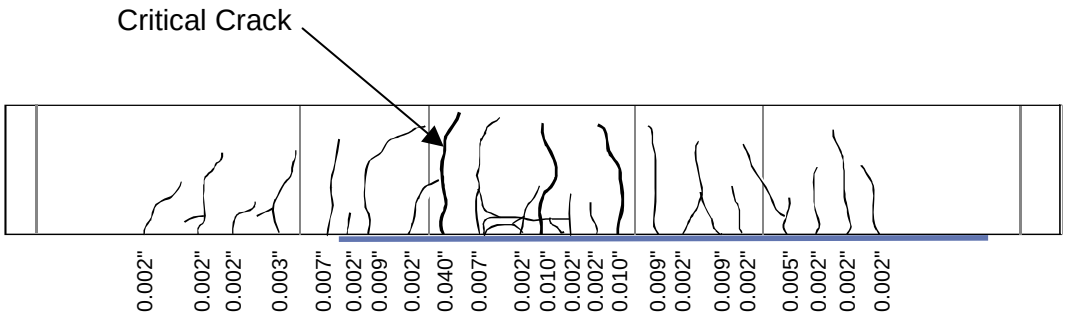

Figure 4.6: Typical Cracking Pattern and Crack Widths Prior to Failure

Figure 4.7: Photograph of Relative Displacement

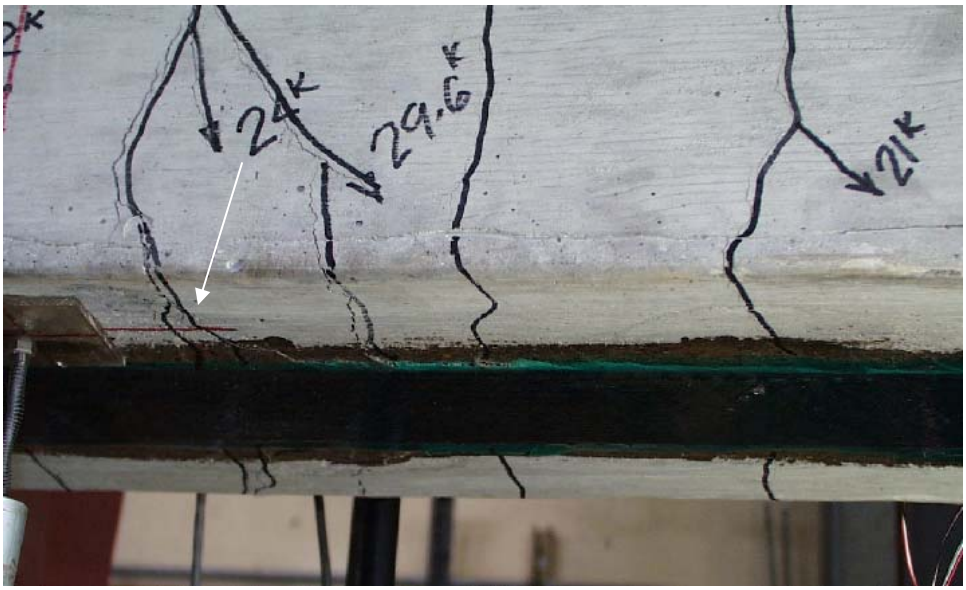

Figure 4.8: Photograph of Debonding Initiated by Prying Action

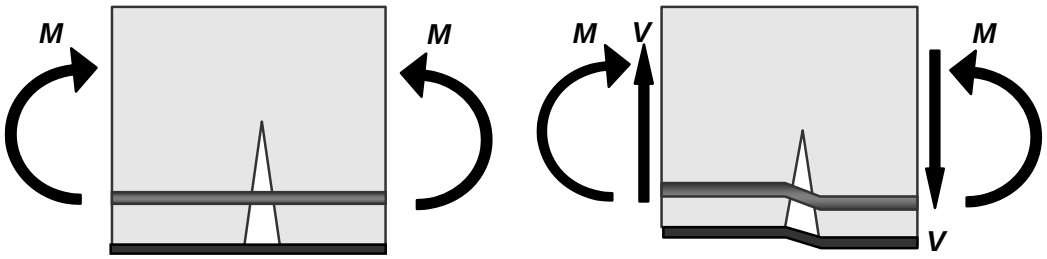

Figure 4.9: Free Body Diagrams of Crack in Constant Moment Region and in Shear Span

In order to achieve the second failure mode, composite rupture, transverse composite straps were provided to prevent debonding failure of the longitudinal composite fibers. Transverse straps allowed the longitudinal composite material to debond locally between straps (Figure 4.10), but maintained sufficient bonded length over the shear span to prevent the debonding failure discussed earlier. Because debonding was prevented at transverse strap locations, the composite was able to reach its rupture strength (Figure 4.11). However, if an insufficient number of transverse straps is provided, the longitudinal composite will still debond and rupture the transverse straps.

Figure 4.10: Debonding Between Transverse Straps

Figure 4.11: Rupture of Composite at Critical Section

4.3.2 Comparison of Measured and Computed Capacity

The ratio of measured to computed capacity, expressed as a percentage, is presented in Figure 4.12 for all strengthened beams. This comparison was made to facilitate comparisons between specimens strengthened with different composite schemes, and to aid in identifying reliable methods for use in design.

Figure 4.12 indicates that only two of the specimens reached the calculated capacity, specimens B2 and B3. However, it must be noted that some of the initial test specimens had bonded composite lengths that realistically could not be expected to develop the strength of the composite. No obvious trend is apparent in Figure 4.12. Trends are more apparent when comparing similar products and application methods. Figure 4.12 will be referenced throughout the chapter in order to make conclusions about the capacities for particular groups of specimens.

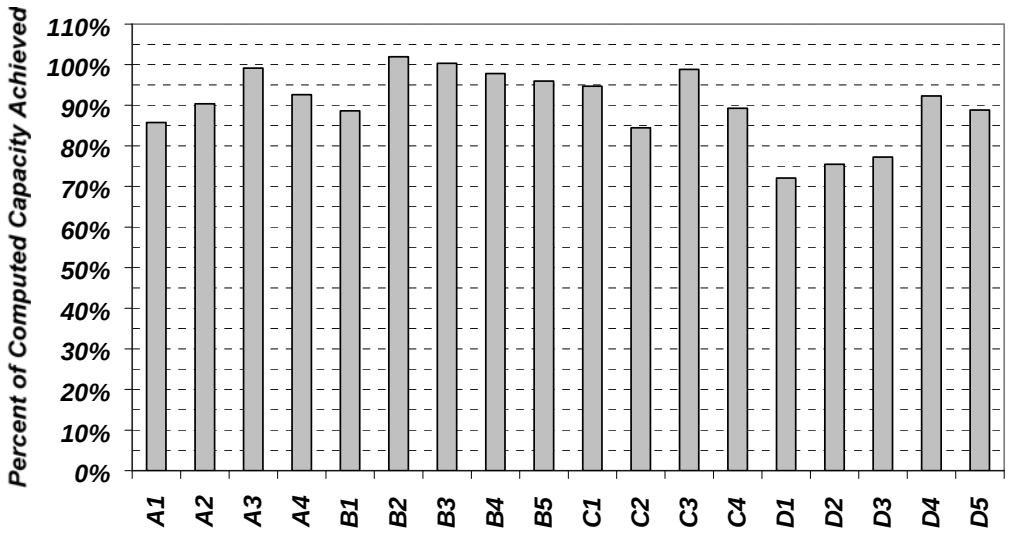

Figure 4.12: Strength Expressed as a Percentage of the Computed Capacity for Each Strengthened Specimen

4.3.3 Strain Ratio

Figure 4.13 compares the strain ratios for all specimens. The strain ratio, which is the ratio of maximum measured strain in the composite to manufacturer-published strain capacity, was calculated to identify values that might be used in design calculations, and to investigate the usefulness of the manufacturer-published strain capacities. There appears to be no general trend among the specimens, aside from the fact that maximum strain in the composite never reached the nominal strain capacity for any composite materials used. However, once again, it must be noted that the bond length used in some specimens (A1 and A2) made it impossible to develop the strength of the composite.

Strain ratios for specimens that experienced composite rupture (these are denoted by hatching in Figure 4.12) ranged from 0.63 to 0.88. Maximum

measured composite strains were unpredictable. Specimens that achieved higher loads sometimes had lower maximum measured strain values in the composite material than specimens that achieved lower ultimate loads. It appears that the published rupture strains overestimate the useful strains in the composites by at least 12%.

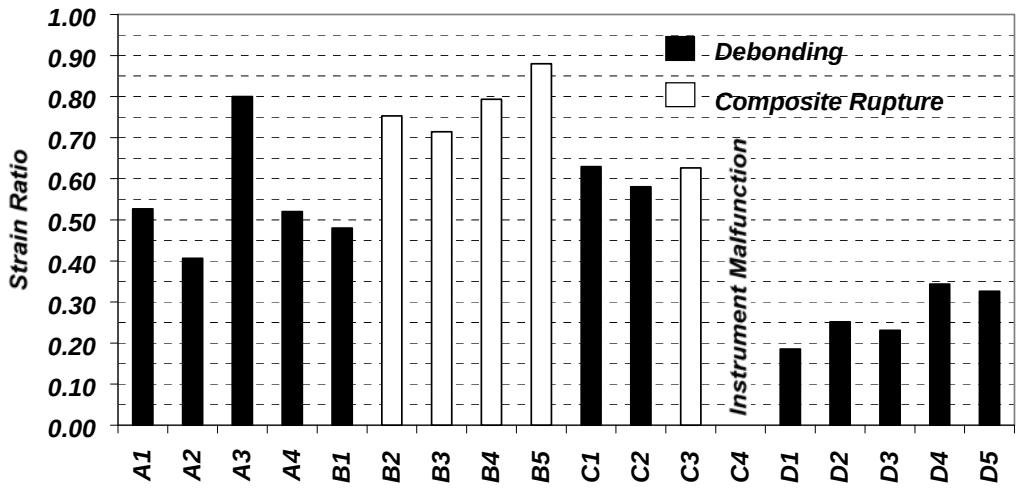

Figure 4.13: Strain Ratio for All Specimens

4.4 EVALUATION OF SPECIMEN BEHAVIOR

Test results from groups of specimens are compared and evaluated in this section. Specific comments about failure modes, percent of computed capacity achieved, displacement ductility factors, and strain ratios are discussed.

4.4.1 Bottom Application

Several different variables were tested with this application to investigate the affect of bonded length, equivalent material from different manufacturers,

nominal bond stress, and surface preparation on the ultimate capacity of the strengthened beams.

4.4.1.1 Bond Length

The first specimen tested, A1, had a bond length of 10 inches (defined in Chapter 3). This specimen performed as expected by debonding of the CFRP as a result of the short bond length. It achieved only 86% of the computed capacity of the strengthened beam because the composite debonded before it could rupture (Table 4.1). Bond length was successively increased after each test that experienced a debonding failure. Specimen A2 had a bond length of 14 inches, and it also debonded at a slightly higher percent (90%) of the computed capacity. The final specimen in this group, A3, had a bond length that extended 30 inches, and it too failed by debonding reaching an even higher load, 99% of the computed capacity.

The load deflection response curves verify that the composite bond length did not affect yield load, as expected. As bond length increased, ultimate load and deflection also increased (Figure 4.14).

As bond length increased, ductility of the strengthened specimen also increased from 1.4 to 1.9 to 3.3 for A1, A2, and A3 respectively (Table 4.1).

The strengthened beams had reduced ductility compared to the unstrengthened beam (Control A&B). Addition of composite material to the beams has the same effect as adding additional tension reinforcement; ductility of the beam is reduced compared to the control beam.

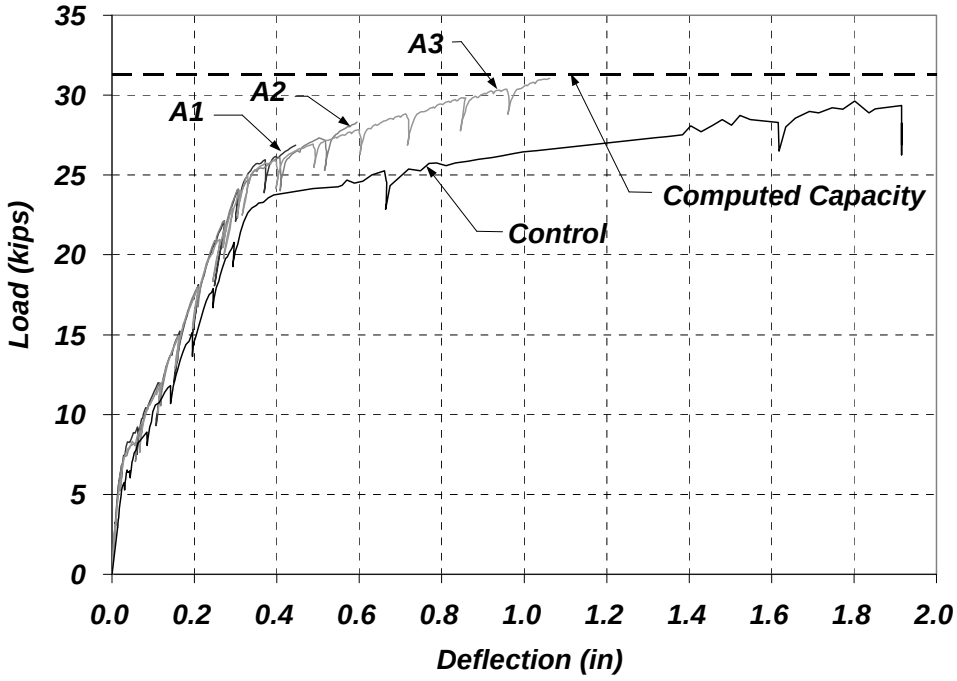

Figure 4.14: Load-Deflection Response for Different Bond Lengths

CFRP strains were measured at the critical section. One would expect that as ultimate load increased, CFRP strains would also increase. However, this was not the case. The strain ratio demonstrates no apparent trend when comparing Specimens A1, A2, and A3 (Figure 4.12). The scatter in Figure 4.13 can be attributed to the unpredictability of the brittle debonding failure. It can also be attributed to the location of the critical crack leading to debonding, which did not always occur at the crack initiator (location of CFRP strain gage).

4.4.1.2 Equivalent Material from Different Manufacturers

Based on the results of the initial bond length tests, the testing program was revised to examine several other factors that could affect the required bond

length. First the A and B systems were compared because the materials were similar. The specified modulus, ultimate strength, and composite thickness of material A were within 97% of the specified properties for material B. Specimen A3 had a bond length of 30 inches and failed by debonding, as mentioned previously. It attained 99% of the computed capacity. Specimen B1 had a bond length of 35 inches and also failed by debonding; it achieved 89% of the computed capacity (Table 4.1).

Specimen A3 reached a higher ultimate load than B1, but B1 exhibited a higher yield load and had greater stiffness after yield than A3. This difference can be attributed to a difference in composite width, which was a construction error. The widths of the composites used to strengthen B1 and A3 were approximately 3 inches and 2 inches, respectively. The area of the composite increased the stiffness and yield load and reduced ductility of specimen B1 as anticipated.

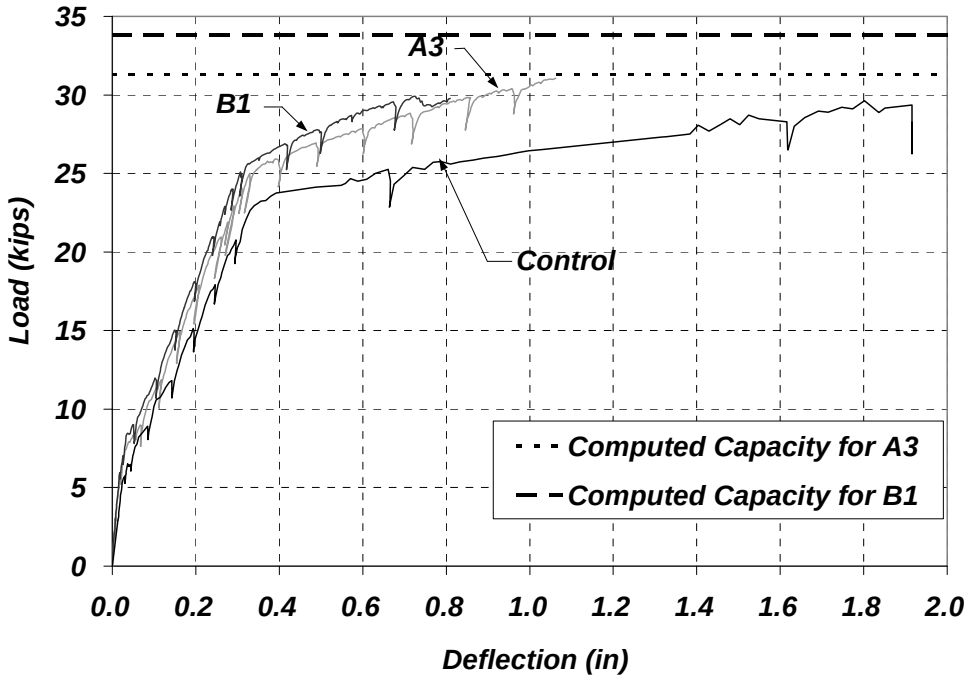

Figure 4.15: Load-Deflection Response for Equivalent Materials

The strain ratio for these two specimens again demonstrates an unexpected trend. There was a substantial difference in the maximum measured strain for the two specimens, even though the bond length was longer for B1. B1 achieved 48% of the published ultimate strain and A3 achieved 80% of the published ultimate strain. This large range in strain ratio can again be attributed to the unpredictability of the debonding failure, which can be a function of the local surface conditions, weakness of the concrete cover, and quality of composite. The failure of B1 at a strain ratio of 48% is all-the-more surprising considering the bonded length was 5 inches longer and the width of the composite was 50% greater than for A3.

4.4.1.3 Equivalent Bond Stress

It was also important to test the manufacturer-recommended bond length equation by varying the width and bond length of the composite while maintaining a constant area of bonded composite. Equation 4-1 was used to determine the bond length required for one ply and two plies of composite.

$$l_{dp} = \frac{f_{pu} t_p n}{3\sqrt{f_c'}} \qquad \text{(Master Builders, 1998)} \qquad (4\text{-}1)$$

l_{dp} = Bond Length (in)

f_{pu} = Composite Rupture Stress (psi)

t_p = CFRP Design Thickness (in)

n = Number of Plies

f'_c = Concrete Compressive Strength (psi)

Because the bonded surface area and nominal cross-sectional area of the composite were the same for both specimens, A3 and A4, the nominal interface shear stress between the concrete and composite and the nominal tensile force in the composite were equivalent for each specimen.

Specimen A3 had a two-ply, 2-inch wide, 30 inch bond length, and it debonded as noted previously at 99% of the computed capacity. Specimen A4 had a one-ply, 4-inch wide 15 inch bond length, and debonded at 93% of the computed capacity (Table 4.1).

These specimens did not perform as anticipated. As shown in Figure 4.16 the load-deflection responses were not equivalent. They not only differed in maximum load achieved, but also ductility. Specimen A3 achieved a higher ductility ratio than A4 (Table 4.1). The results indicate that the bond stress

equation recommended by one manufacturer is not sufficient to describe the behavior of CFRP bonded to the surface of reinforced concrete beams.

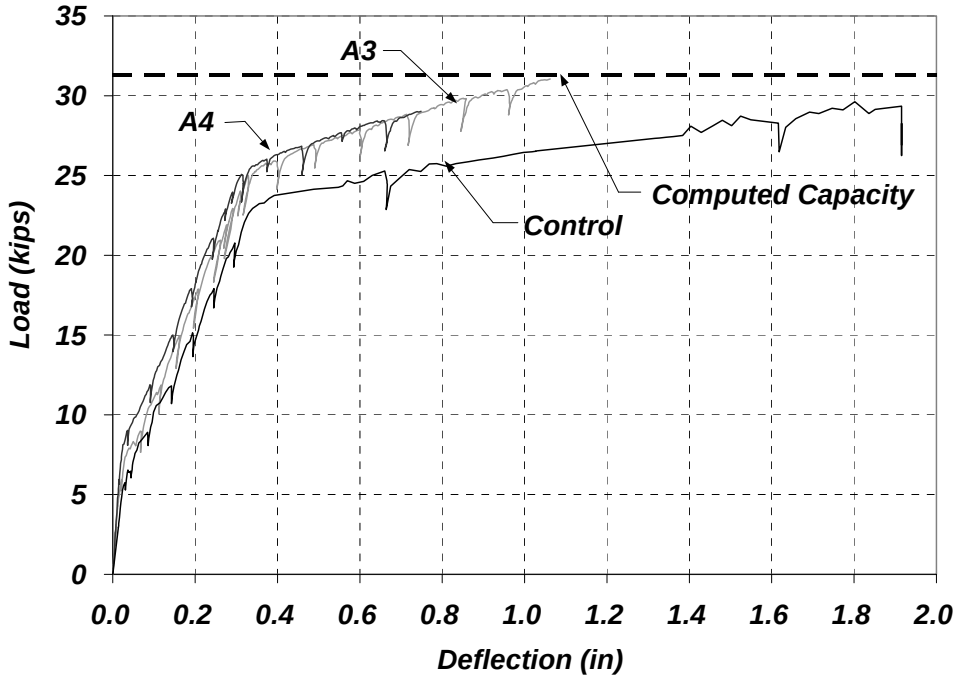

Figure 4.16: Load-Deflection Response for Equivalent Bond Stress

The strain ratio for A4 (52%) was substantially less than the ratio for A3 (80%). The shorter bond length used for specimen A4 might have been more susceptible to prying action than the longer length used in specimen A3.

4.4.1.4 Influence of Surface Preparation

The larger beams (both longer span and deeper cross-section) in this group strengthened with systems C and D were tested first with the maximum bond length possible, 45 inches. Specimens C1 and D1 also failed by debonding at 95% and 72% of the computed capacities. Because the specimens debonded

while investigating the maximum bond length, the influence of surface preparation was chosen as the next variable to investigate. Previous specimens were all prepared by grinding the concrete surface, so C2 and D2 were prepared by sandblasting. The effects of surface preparation were difficult to interpret because sandblasting decreased the capacity of the C system and slightly increased the capacity of the D system (Figures 4.17 and 4.19). Differences might be attributed to the composite system used: wet lay-up for system C, versus pultruded for system D.

Specimen C2 achieved 84% of the computed capacity, and specimen D2 achieved 75% of the computed capacity (Table 4.1).

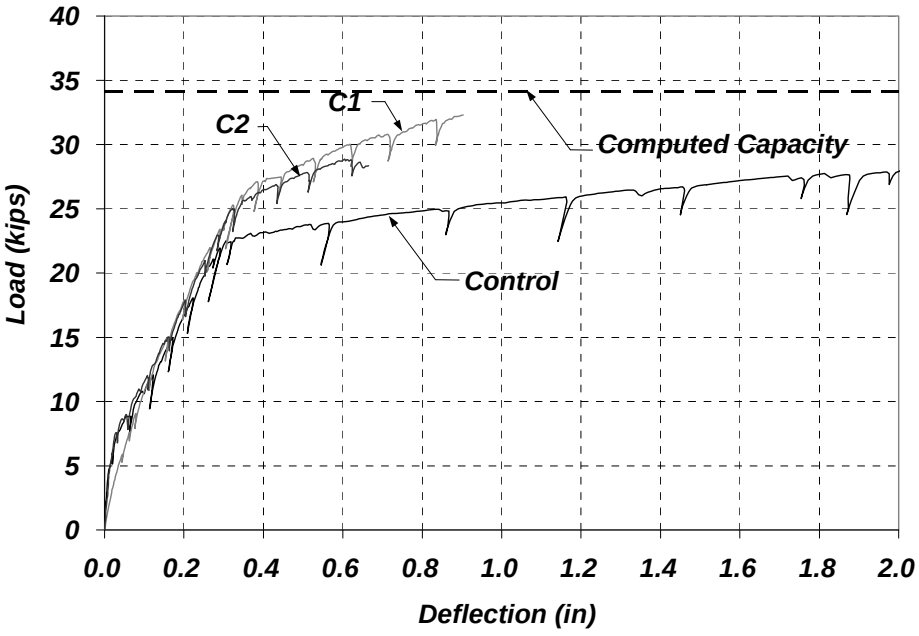

Figure 4.17: Load-Deflection Responses for C System Surface Preparation

Reduction in bond capacity (and specimen capacity) for the wet layup system when the surface of the concrete was prepared by sandblasting was evident in the appearance of the concrete surface after failure. A typical specimen with poor composite bond is shown in Figure 4.18, the concrete surface was smooth. Specimens with this failure surface were indicative of inadequate bond between the composite and concrete.

Figure 4.18: Evidence of Poor Composite Bond

Unlike the C system, the D system was a pultruded composite, and sandblasting slightly improved the behavior of this system (Figure 4.19). Specimen D1 achieved 72% of the computed capacity while D2 achieved 75% of the computed capacity (Table 4.1). The results indicate no clear improvement in bond due to sandblasting. The percent of computed capacity achieved for this

system was low compared to the other systems discussed thus far. Once again, failure by debonding was sudden and without warning.

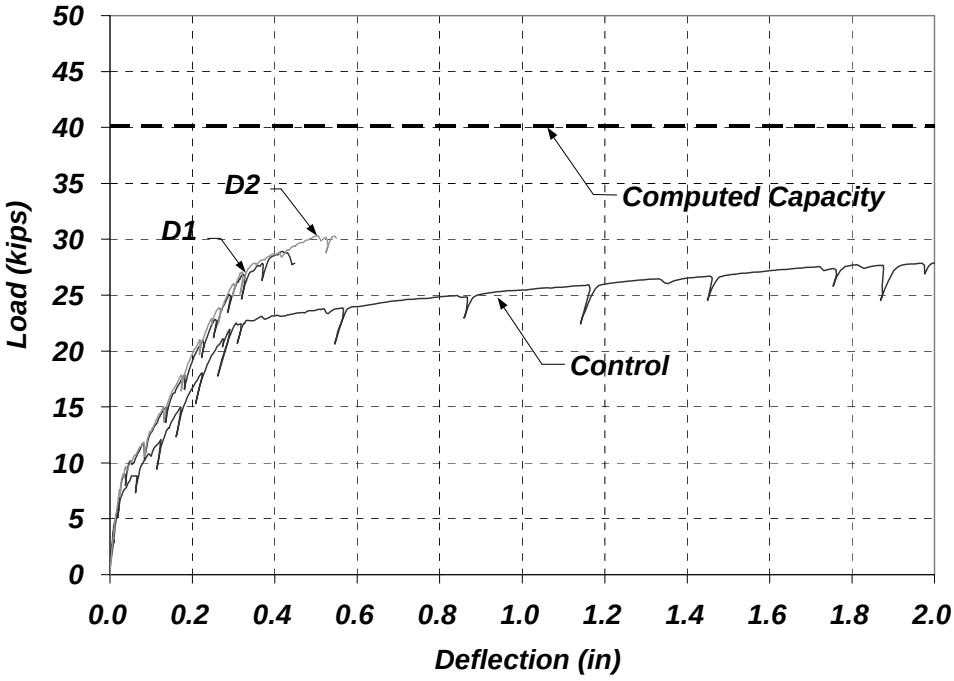

Figure 4.19: Load-Deflection Responses for D System Surface Preparation

For the D system the maximum measured strains were very low compared with the published rupture strain. D1 reached only 19% of the published strain and D2 reached 25% of the published strain (Table 4.1).

The slight increase in strength was also evident in the appearance of the concrete and composite surface after failure. As shown in Figure 4.20 for a typical specimen with good composite bond, the concrete surface was rough. This failure surface suggests good bond between the composite and concrete and is significantly different than that shown in Figure 4.18 for poor composite bond.

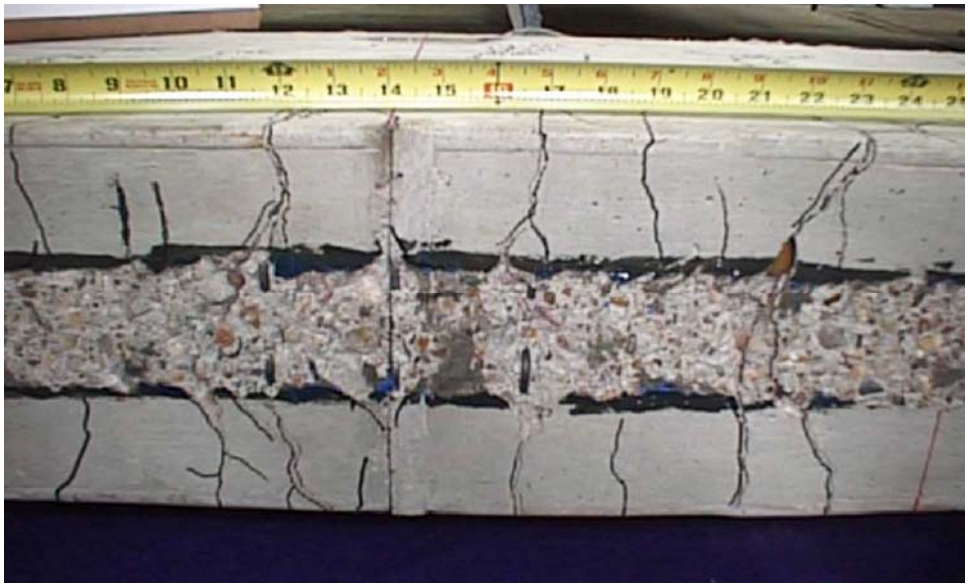

Figure 4.20: Evidence of Good Composite Bond

There are many other factors that affect the effectiveness of the material more significantly than surface preparation, such as, high shear stress in the concrete, high interface shear stress between the concrete and composite, inadequate anchorage, and weakness of concrete cover. The remainder of the specimens were prepared by grinding the surface of the concrete.

4.4.1.5 Summary

All of the specimens with CFRP applied to the bottom surface of the concrete failed by debonding, which leads one to believe there is no "development length" for the beam lengths tested that will fully engage the strength of the composite fibers. The debonding failure was very sudden and brittle. It was initiated by the relative vertical displacement that occurred at crack locations. As the bond length increased, the load and displacement also increased

as expected. However, the failure was unpredictable and did not correspond with the idealized behavior. Debonding failure prevented the strength of the composite material from being developed.

4.4.2 Bottom Application with Transverse Straps

This application required use of a wet lay-up system for the transverse straps. Two wet lay-up composite systems, B and C, were tested with this application. The variables tested in this group were the bond length of the longitudinal composite and the number of straps provided along each shear span.

The tests performed indicated that as the bond length increased, capacity and ultimate deflection increased; and the capacity increased as the number of straps increased for a given length of longitudinal CRFP material. This set of tests also demonstrated improved ductility. As peak load was approached, the composite exhibited evidence of distress through cracking and popping sounds, whitening of epoxy in the vicinity of cracks, debonding between transverse straps, and debonding of transverse straps (Figure 4.21). These were all signs that the system was reaching its limit. Once ultimate load was attained, failure was very sudden and violent when the longitudinal composite ruptured.

Figure 4.21: Debonding of Strap

4.4.2.1 B System

Two specimens were used for comparison in this set of tests: the unstrengthened specimen and specimen B1 with the composite bonded to the bottom of the beam with a 35 inch bond length. Three specimens were tested with transverse straps: B2, B4, and B5. B2 had the composite bonded the maximum length of 35 inches and had straps spaced at h/2 along the full length of the shear span (seven straps). B4 had the same layout as B2, except straps were only placed along half the shear span (four straps). Specimen B5 had a bond length of 24 inches and straps spaced at h/2 along half the shear span (four straps).

B2 exhibited the best performance of the three specimens with transverse straps (Figure 4.22). It achieved 102% of the computed capacity and a displacement ductility of 3.3 (Table 4.1). Specimen B4 had the next best

performance reaching a similar ductility of 3.4 but a lower ultimate load (98% of the computed capacity) than B2. Specimen B5 was inferior to both B2 and B4 with a capacity that was 96% of the computed capacity and a ductility ratio of 2.9. Specimens B2, B4, and B5 with transverse straps achieved higher ultimate loads that were closer to the computed capacity than the specimens that failed because of composite debonding, such as B1 (Table 4.1).

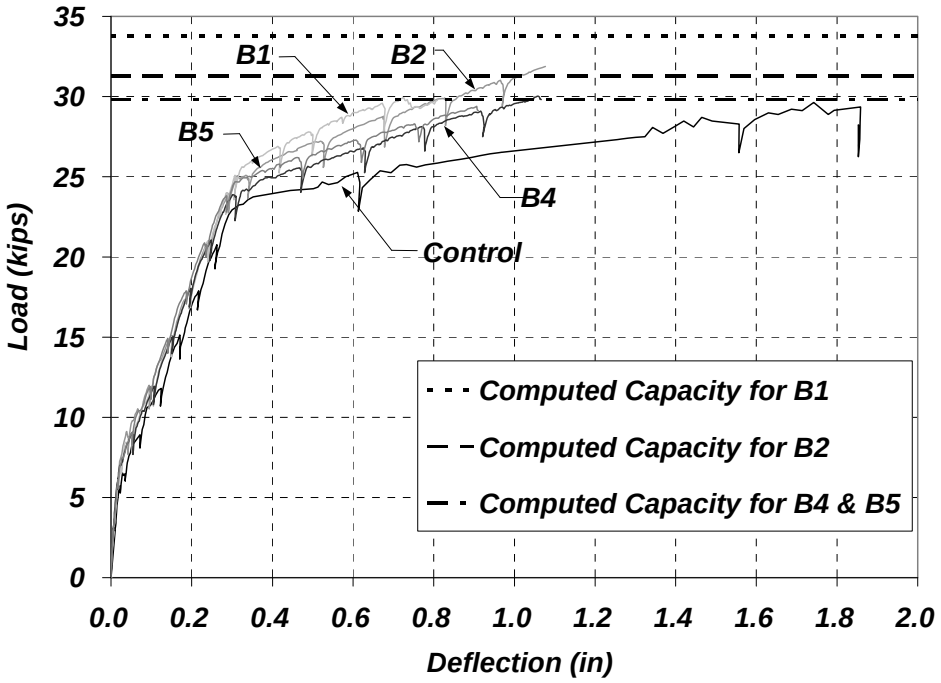

Figure 4.22: Load-Deflection Response for B System Beams with Transverse Straps

Strain ratio values ranged from 75% to 88% of the published ultimate strain (Figure 4.13). The scatter associated with these strain ratios was substantially less than for specimens where composite debonding occurred.

4.4.2.2 C System

For the C system, only one specimen, C3, was tested with the transverse straps, and its response was compared to the unstrengthened specimen and specimen C1 with no transverse straps. Specimen C3 had a 45 inch bond length and transverse straps at h/2 spacing along the full shear span (seven straps). It reached 99% of the computed capacity, and failure was governed by composite rupture (Table 4.1). C3 also achieved a slightly higher displacement ductility than C1 (2.9 versus 2.7).

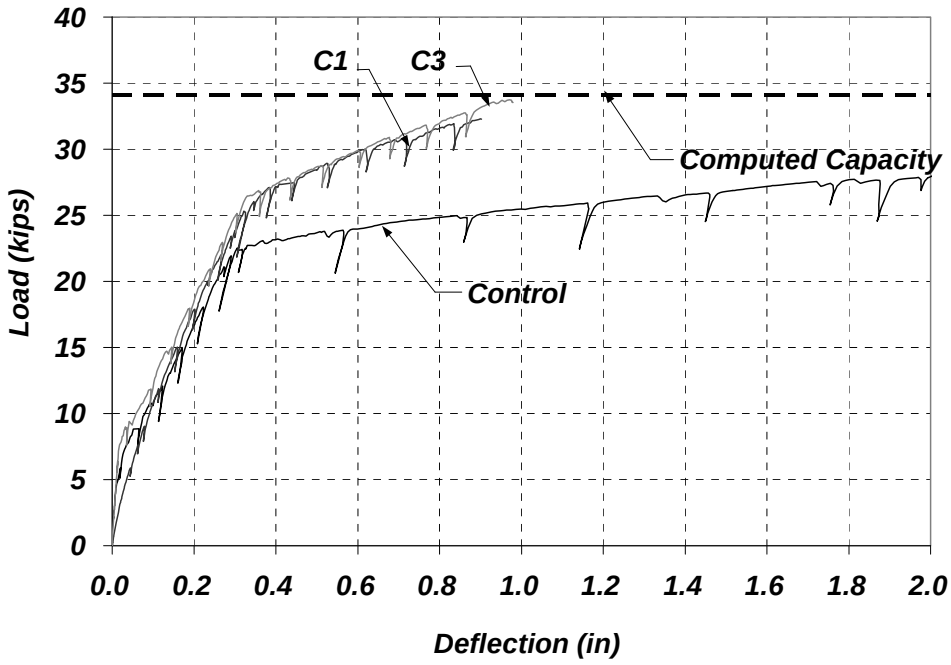

Figure 4.23: Load-Deflection Response for C System with Transverse Straps

Strain ratios were unexpectedly the same for these two specimens (Figure 4.13). It was expected that C3 would have achieved a slightly higher maximum strain than C1 because of the higher load achieved by C3.

4.4.2.3 Summary

This group of tests demonstrated that fracture of longitudinal composite material was possible with the addition of transverse straps. The composite ruptured in every specimen at the critical section. Not only was maximum load increased, but displacement ductility was also enhanced in these specimens. There was also significant warning leading up to failure. Popping and cracking sounds, debonding between transverse straps, and debonding of portions of some of the transverse straps, preceded failure.

Rupture of the composite did not guarantee achieving the published ultimate composite strain. For these specimens the highest strain ratio was 0.88. Strain measurements made at the critical section at yield and at ultimate for the two best-behaved specimens in this group (B2 and C3) are shown in Figure 4.24. The strain plots indicate that composite strains at ultimate are substantially less than would be expected if plane sections remained plane up to failure. This is likely due to debonding of the composite between transverse straps resulting in measured strains that reflect the total deformations between two straps divided by the distance between those two straps.

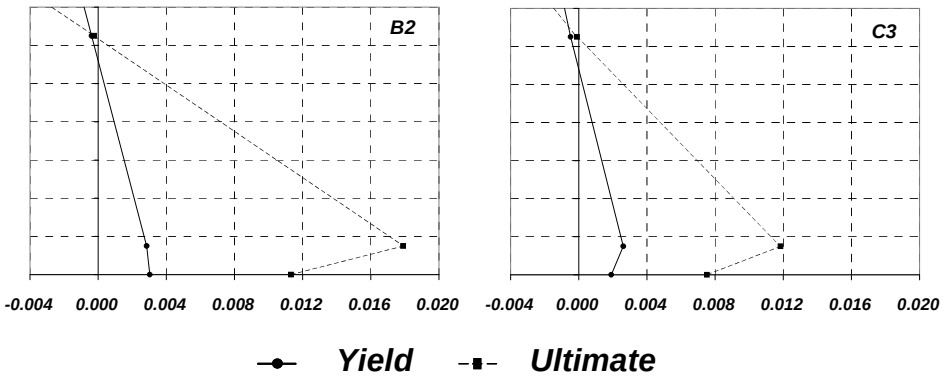

Figure 4.24: Strain Profiles at Yield and Ultimate for Specimens B2 and C3

4.4.3 Side Application

This application exhibited similar failure characteristics as for earlier bottom-application specimens. One notable similarity was the manner in which cracks propagated parallel to the composite as debonding initiated after yield and prior to failure (Figure 4.25). Flexural cracks divided into several cracks in the vicinity of the composite.

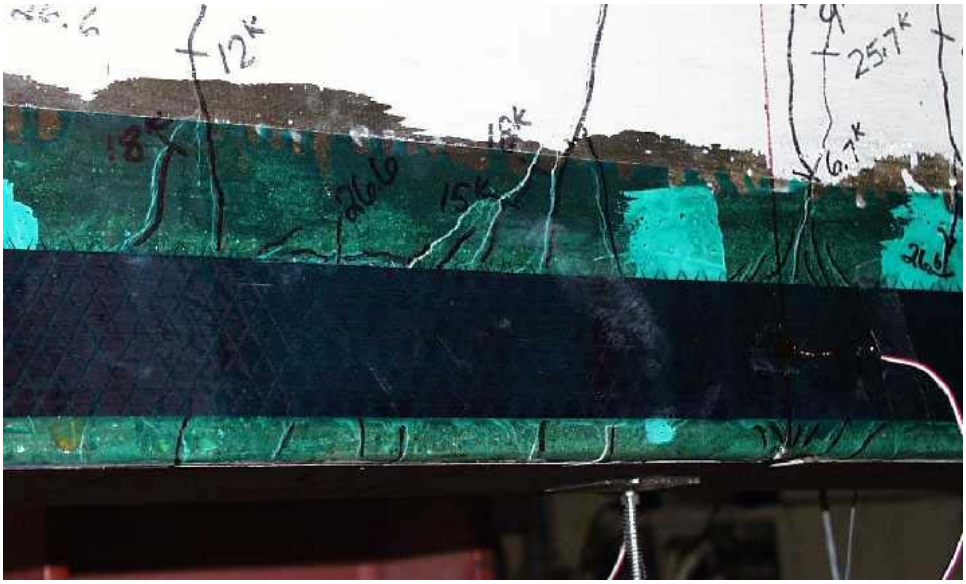

Figure 4.25: Typical Cracking Associated with Side Application

This application was tested using both wet lay-up and pultruded composites. Three systems were tested: B, C, and D. The only variable considered in this group was the location of the primary composite, bottom of beam versus side of beam. The depth of the composite was approximately 1 ½ in. less for the side application than for the bottom application. All composites were bonded the maximum length that could be accommodated by the span.

The load capacities achieved by beams with side application were slightly lower than beams with bottom application because the composite was not bonded to the extreme tension fiber of the beams. The reduced moment arm resulted in reduced capacity. However, this did not affect the deformation capacity of the strengthened beams.

4.4.3.1 B System

Specimen B3 had a bond length of 35 inches on the sides of the beam. Response of B3 is compared to the beam B1 with the composite bonded to the bottom of the beam and with a 35 inch bond length, and B2 with the composite bonded the maximum length of 35 inches and transverse straps spaced at h/2 along the full length of the shear spans.

The load-deformation response of B3 is similar to that for B2 (Figure 4.26). Specimen B3 achieved 100% of the computed capacity and failed by composite rupture (Table 4.1). Maximum measured composite strain was 71% of the published strain (Table 4.1).

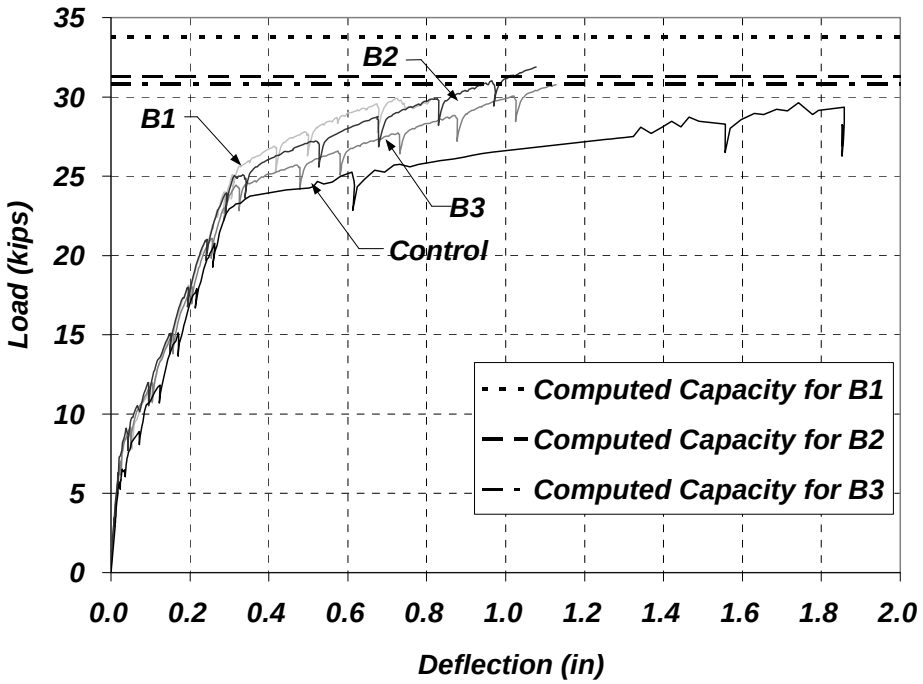

Figure 4.26: Load-Deflection Response for B System Side Application

Figure 4.27 illustrates the failure of this specimen. Not only did the composite rupture, but concrete cover was also pulled off during failure.

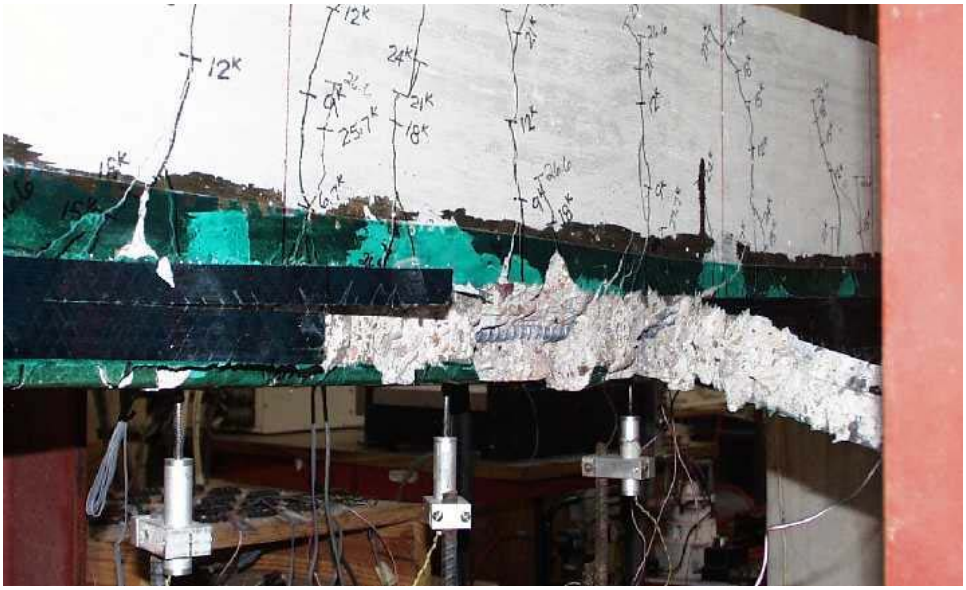

Figure 4.27: Specimen B3 at Failure

4.4.3.2 C System

Specimen C4 had a bond length of 45 inches on the sides of the beam, which was the maximum possible length. Response is compared to the response of beam C1, with the composite bonded to the bottom of the beam with a 45 inch bond length, and the response of C3, with a bond length of 45 inches and transverse straps spaced at h/2 along the full length of the shear spans.

Specimen C4 achieved a smaller load (89% of computed capacity) than both C1 and C3 (Figure 4.28). Deformation capacity was similar to that for C1 and C3. C4 failed by debonding (Figure 4.12). However, the capacity and ductility for C4 were reasonably close to the same capacity and ductility as for

C3, which failed by rupture of the composite material. This suggests that the composite in C4 may have been very close to rupture.

Strain in the composite is not known for C4 because of an electronic malfunction in the data acquisition equipment.

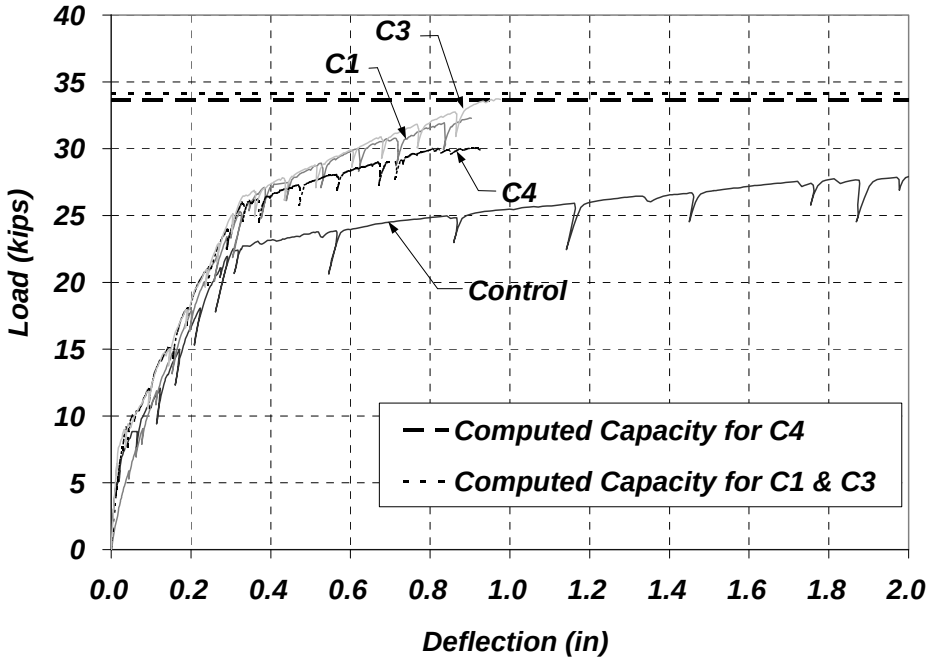

Figure 4.28: Load-Deflection Response for C System Side Application

4.4.3.3 D System

Specimen D3 also had a bonded length of 45 inches on the sides of the beam. Its response is compared to the response of the unstrengthened beam, Contol C &D, and the strengthened beam D1 with the composite bonded to the bottom of the beam with a 45 inch bond length. The pultruded plates used to strengthen D1 and D3 were only available in certain widths and thicknesses, so

the area of composite was not equal for these specimens, unlike the other side-application specimens. D3 had twice as much composite bonded as D1 because it had two plies bonded to the sides (one on each side) instead of one bonded to the bottom of the beam.

Specimen D3 performed well compared to D1, although it also failed by debonding (Figure 4.28). It had a much higher yield and ultimate load than D1. The yield load and post-yield stiffness were greatly increased for specimen D3 because it had twice the amount of composite bonded that D1 had (Figure 4.30). Specimen D3 achieved 77% of the computed capacity, which was slightly better than D1 which attained 72% of the computed capacity (Figure 4.12). The strain ratio was again low at 23% of the published strain value. This system did not make efficient use of the composite, which was controlled by debonding failure.

Figure 4.29 illustrates the failure. Not only did the composite debond, but also concrete cover spalled off during failure. This indicates that debonding was a function of the tensile capacity of the concrete instead of the tensile strength of the epoxy.

Figure 4.29: Specimen D3 at Failure

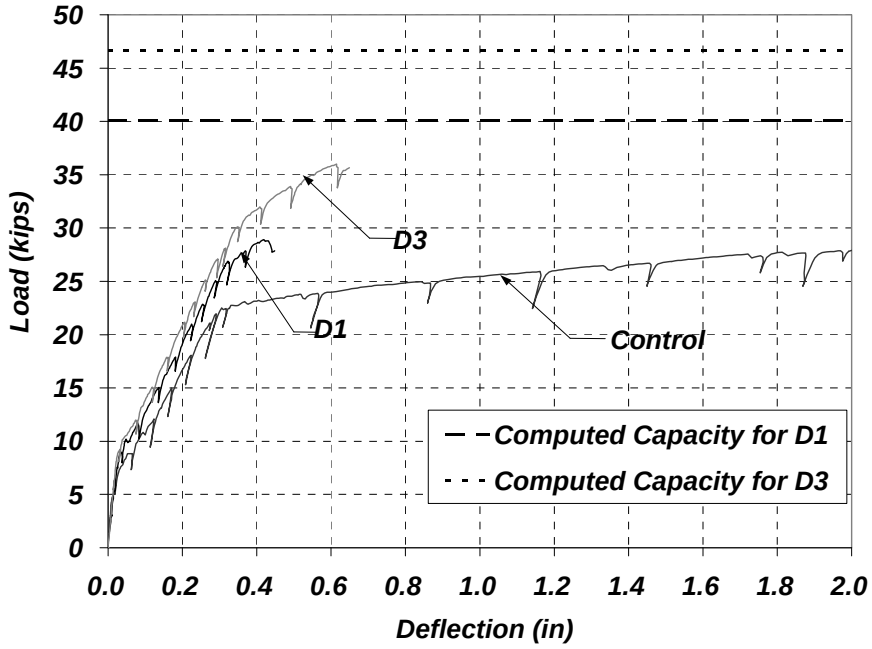

Figure 4.30: Load-Deflection Response for D System Side Application

4.4.3.4 Summary

Side application of the composite generally produced behavior that was superior to comparable specimens with bottom application of the composite. In one case (B3) the composite ruptured, and in others the composite debonded from the beam. Even specimen C4 that failed by debonding was very close to reaching the same load achieved by the bottom application with transverse straps because it was not affected by the vertical offset at the critical crack location. The results from the specimens with B and C systems were acceptable because the percent of computed capacity was quite high and strain ratios approached the published values. The performance of the D system still was quite inefficient because the system was debonding prematurely.

Not enough specimens were tested to recognize trends in bond length, surface preparation, etc. for this application method. However, it could be inferred that it is possible to attain the capacity of the wet lay-up system, and performance is generally better than for bottom-application specimens. The pultruded system did not benefit substantially from the side application alone.

4.4.4 Side Application with Transverse Straps

One more application scheme, side application with straps, was attempted because the D system (utilizing pultruded plates) did not reach the computed capacity for any of the tests described earlier. This application was only tested for the D system. In the previous group of tests, the D system pulled off large pieces of concrete cover and exposed steel reinforcement when it debonded. This application was similar to the previous transverse strap application except an

attempt was made to not only anchor the composite but also the concrete because debonding appeared to be a function of the concrete tensile strength.

The two specimens with transverse straps, D4 and D5, did not achieve the computed capacity because the composite debonded after transverse straps ruptured. However, the results were improved from those for the specimens without transverse straps. The straps, made of wet lay-up composite E, were not sufficiently strong to prevent the composite from debonding (Figure 4.31). The specimen with the best performance, D4, had a maximum bond length for the composite of 45 inches and had transverse straps spaced at h/2 along the full length of each shear span (Figure 4.32 and Table 4.1). It achieved 92% of the computed capacity, and a displacement ductility of 2.6. Specimen D5 displayed a slightly lower ductility and ultimate load (89% of the computed capacity) than D4. D5 had a bond length of 30 inches, and the transverse straps were spaced at h/2 along half of each shear span. Even though these specimens failed by debonding, they achieved higher loads that were closer to the computed capacity than specimens that did not have transverse straps to enhance anchorage (Figure 4.12).

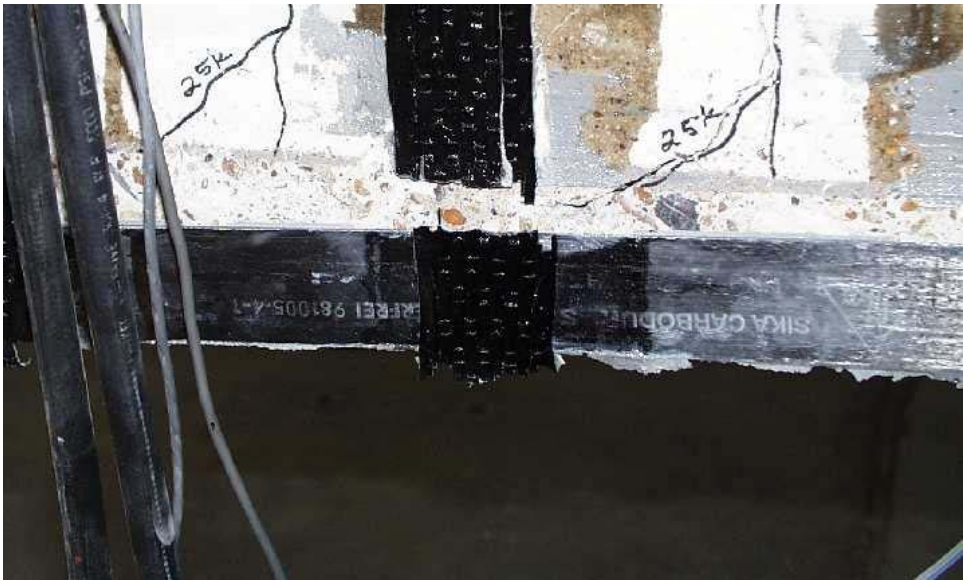

Figure 4.31: Debonding Failure with Strap Rupture for Specimens with Side Application with Straps

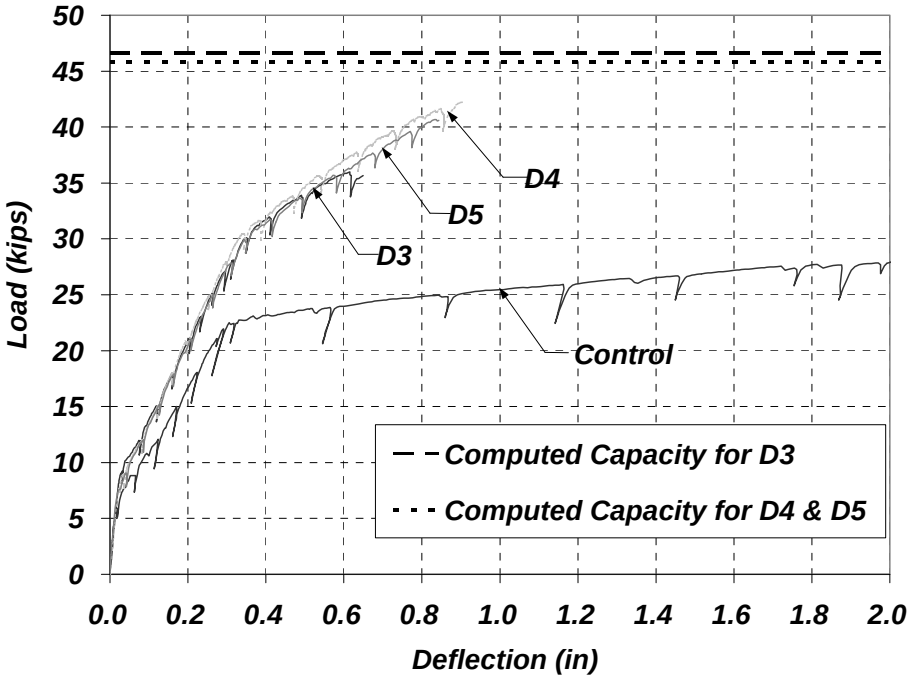

Figure 4.32: Load-Deflection Response for D System Side Application with Transverse Straps

Strain ratio was again very low at 33% of the expected strain value (Table 4.1). This system, which is controlled by debonding failure, makes inefficient use of the composite material. However, the percent increase in strength obtained over the control specimen is substantial for this system. Pultruded plates with smaller cross-sectional area would likely be far more efficient.

Although results were improved with the transverse strap application, the D system still was inferior to the other systems in terms of efficiency of material use and failure mode. The transverse straps were beneficial to the performance of the system. Similar to the bottom application with transverse straps, a greater bond length and number of straps resulted in improved performance.

The system also demonstrated improved warning before failure. Popping and cracking sounds, debonding between transverse straps, and debonding of small portions of the transverse straps preceded failure.

4.4.5 Recommended Application Methods

From the previously described test results, it can be concluded that the preferred application method is one that utilizes transverse straps to improve anchorage of the primary composite to steel-reinforced concrete beams. Of the two application methods with transverse straps, bottom application with transverse straps was the only scheme that consistently promoted rupture of the longitudinal composite at failure. However, side application of the wet lay-up system with transverse straps was not tested.

For specimens strengthened using the B composite with bottom application and transverse straps (B2, B4, and B5), the average maximum CFRP strain was 0.012 (Figure 4.33). This is approximately 80% of the manufacturer-published 0.015 CFRP strain capacity. It is believed that the A system would have performed similarly to the B system because the materials had virtually the same material properties, as noted in Chapter 3.

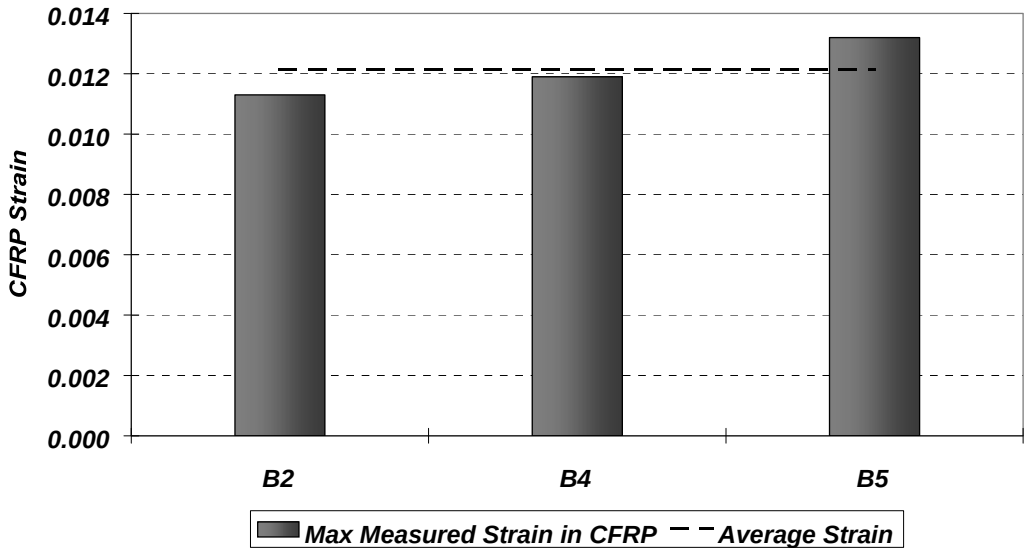

Figure 4.33: Average CFRP Strain at Rupture for the B Composite System and Bottom Application with Transverse Straps

For the specimen strengthened using the C composite with bottom application and transverse straps (C3), the maximum CFRP strain was 0.0075. This is only 63% of the manufacturer-published CFRP strain capacity of 0.012.

The D system was the only composite tested that never ruptured during testing. However, the behavior improved significantly when the composite was applied on the sides of the beams and transverse straps were used to improve anchorage. It is believed that if the pultruded plates had been tested in this manner with less material in the composite cross section, rupture of the pultruded plates would have occurred. This was not attempted because the pultruded plates used in the study were only available in the widths and thicknesses tested.

For specimens strengthened using the D composite with side application and transverse straps (D4 and D5), the average maximum CFRP strain was 0.0064

(Figure 4.33). This is only 33% of the manufacturer-published CFRP strain capacity of 0.019.

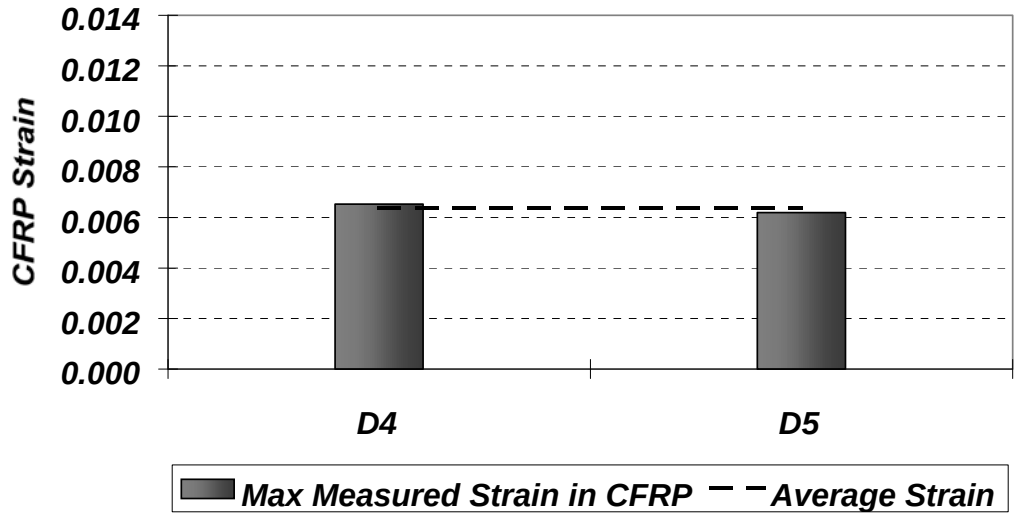

Figure 4.34: Average CFRP Strain for the D Composite System and Side Application with Transverse Straps

Chapter 5: Summary and Conclusions

5.1 Overview of Test Program

The testing program included twenty rectangular reinforced concrete beams that were loaded monotonically to failure. Eighteen of the beams were strengthened using carbon fiber composites and two beams served as control specimens. Observed modes of failure corresponded with composite debonding, composite rupture, or concrete crushing.

Beam specimens were 8”x14”x 9’-6” and 8”x16”x 10’-6” with longitudinal reinforcement ratios of 0.62 and 0.53%, respectively. The smaller beams were strengthened using two different wet lay-up CFRP systems, and the larger beams were strengthened using a wet lay-up CFRP system and a pultruded CFRP system. Four strengthening schemes, including bottom application, bottom application with transverse straps, side application, and side application with transverse straps, were investigated. Findings from each group of tests are summarized in the following section. The matrix of tests performed in this study is summarized in Table 3.1, the identities of suppliers of the carbon fiber materials used to strengthen beams are provided in Section 3.5.3.2, and material properties are presented in Table 3.6.

5.2 SUMMARY OF TESTS

5.2.1 Bottom Application of Composite Material

Composite material was bonded over various lengths of the bottom surface of the beam in an attempt to determine the bond length needed to result in rupture of the composite material at beam failure. Bond length varied from a minimum of 10 in. to a maximum of 35 in. (bond length is defined in Section 3.2.2.1) for the smaller beams, and was the maximum possible length (45 in.) for the larger beams. In addition to bond length, different layouts with equivalent nominal interface shear stress, and different surface preparations (grinding vs. sandblasting) also were studied.

Following is a summary of results from the tests of beams with bottom application of the composite material:

(1) Longer bond lengths increased strength and deformation capacity of strengthened beams relative to that for the beam with the shortest bond length. None of the specimens with the composite applied to the bottom surface of the beam experienced rupture of the composite material; all experienced sudden debonding of the composite. Differential vertical displacements across a critical flexure-shear crack pried the composite from the surface of the concrete in the vicinity of the crack and initiated debonding of the composite material in each test.

(2) The capacity of beams strengthened with wet lay-up systems ranged from 84 to 99% of the computed capacity. The capacity calculation was based on the assumption that rupture of the composite material would control failure of the

strengthened beams. Maximum measured strains at failure ranged from 0.0061 to 0.0120, which was 41 and 80% of supplier-specified rupture strains for the respective materials.

(3) The capacity of two beams strengthened with pultruded plates ranged from 72 to 75% of the computed capacity, and the maximum measured composite strains at failure ranged from 0.0035 to 0.0048. The strengths and maximum composite strains, which were low compared with values from the wet lay-up specimens, are likely related to the relatively large quantity of composite material that was attached. Pultruded plates were available in limited widths and thicknesses that were too large for the beam cross sections tested in this study. However, the debonding failures experienced in this study indicate that it will likely be difficult to keep the pultruded plates attached to larger beams up to failure.

(4) The influence of the composite layout was examined by comparing the behavior of a beam strengthened with two plies of 2-in. wide composite strip having a 30 in. bond length to the behavior of a beam strengthened with one ply of 4-in. wide composite strip having a 15 in. bond length. Because the surface area and nominal cross-sectional area of the composite were the same for both specimens, the nominal interface shear stress was the same. The strength of the specimen with the 15 in. bond length was approximately 93% of the strength of the specimen with the 30 in. bond length. The maximum composite strain was significantly smaller (0.0078 vs. 0.0120) and ultimate deflection was smaller (0.75 vs 1.06 in.) for the shorter bond length. The shorter bond length might have

made the composite more susceptible to debonding after debonding was initiated by prying at the critical crack.

(5) The influence of surface preparation on composite bond strength was studied using two pairs of beams that were fabricated to be nominally the same, with the exception of surface preparation. In each pair, grinding (the surface preparation technique used for almost all specimens) was used to prepare the bottom surface for composite bonding on one beam and sand blasting was used to prepare the bonding surface of the second beam. For one pair of beams, a wet lay-up system was used, and for the other pair, the pultruded system was used. For both composite systems, the maximum available bond length (45 in.) was used. No clear trend was observed from tests on the two sets of specimens. For the wet lay-up system, strength and deformations were reduced when sandblasting was used for surface preparation. For the pultruded system, a slight increase in strength and deformations was observed.

5.2.2 Side Application of Composite Material

Three beam specimens were strengthened with longitudinal composite strips applied to the side faces of beams. Side application was investigated to determine if the composite material was affected less by vertical offsets at critical flexure-shear cracks. Two wet lay-up systems and the pultruded system were examined. Longitudinal strips were applied with the maximum bond length available for all specimens. The following observations were made:

(1) One wet lay-up specimen developed the computed strength and experienced composite rupture. The other wet lay-up specimen failed as the

result of composite debonding. Strength of the specimen that experienced composite rupture exceeded the strength of a companion specimen with bottom application of the composite. This has additional significance because the composite material used in the side application was located at a smaller effective depth than when applied to the bottom surface. Deformations for both specimens with side application of the composite were equal to or larger than deformations for companion specimens with composite material applied to the bottom of the beams.

(2) The specimen strengthened with side application of pultruded strips failed as the result of composite debonding. The failure load was 25% greater than the companion specimen with composite material applied to the bottom surface, although the ratio of measured capacity to computed capacity was similar (77% for side application and 72% for bottom application). Additional capacity for the side-application specimen was due to the larger quantity of carbon-fiber used to strengthen the beam. Twice the quantity of pultruded plate was used for the side-application specimen because smaller pultruded strips were not available from the material supplier. Maximum measured deflection and composite strain were 48 and 26% larger for the specimen with side application of the composite.

5.2.3 Addition of Transverse Straps

Transverse straps spaced at h/2 were added to improve anchorage of the longitudinal composite strips, and thus, to delay debonding or facilitate rupture of the longitudinal strips. The following observations were made from tests incorporating transverse straps:

(1) Transverse straps applied to beams strengthened with two different wet lay-up systems applied to the bottom surface of the beams resulted in fiber rupture for all beams, and strengths that varied from 96 to 102% of the computed capacity. Deflections at ultimate strength were from 9 to 47% larger than the maximum deflections measured for companion specimens with composite material applied to the bottom surface of the beam.

(2) Beams strengthened with pultruded strips applied to the sides of beams and wet lay-up transverse straps experienced debonding failures. Strengths were 13 and 18% higher than the strength of the companion beam with only longitudinal strips applied to the beam sides. Deflections at failure also increased by 36 and 47%.

(3) Beams with transverse straps applied over the half of each shear span adjacent to the constant moment region developed slightly lower capacities (less than a 7% reduction) and slightly smaller deflections at failure (less than an 8% reduction).

(4) Reduced bond length (from 35 to 24 in.) for one of the wet lay-up systems applied to the bottom surface of the beam in conjunction with the reduced number of transverse straps resulted in further reduction in strength and deformation capacity (8.5 and 19%, respectively).

5.3 RECOMMENDATIONS

The results of this study conclude that CFRP systems are a viable option for strengthening reinforced concrete beams. Based on the carbon fiber

composite strengthening program described here, which was limited in scope to rectangular beam sections, the following recommendations are made:

(1) For more consistent behavior, longitudinal composite strips should have the maximum available bond length, and be accompanied by transverse straps spaced at h/2 over entire shear spans.

(2) Although strain measurements indicated a lack of compatibility between fiber composites and the reinforced concrete section as failure was approached, calculated capacities of beams strengthened with wet lay-up systems having transverse straps can be computed conservatively using a maximum fiber strain of 0.0075. Three of the four specimens tested with wet lay-up systems and transverse straps experienced maximum measured strains of at least 0.011.

(3) Calculated capacities of beams strengthened with pultruded plates having wet lay-up transverse straps can be computed conservatively using a maximum fiber strain of 0.006. It is likely that larger strains could be developed if a relatively lower ratio of plate material were used.

(4) All beams were loaded with a symmetrical two-point load. Behavior of strengthening schemes should be investigated for non-symmetrical load distributions that are representative of various design bridge loads.

Appendix A: Cracking Patterns

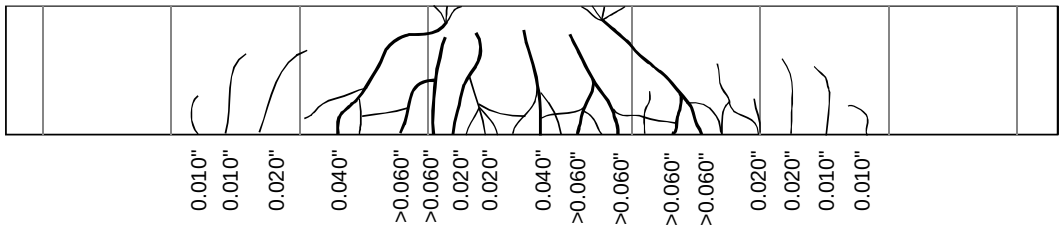

Control A & B

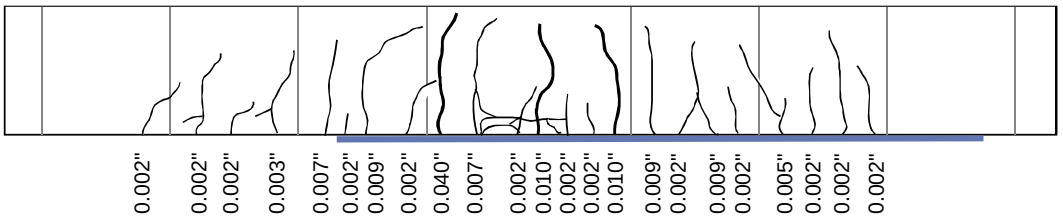

A1

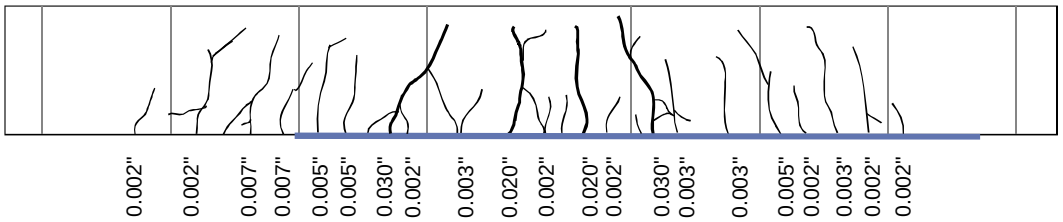

A2

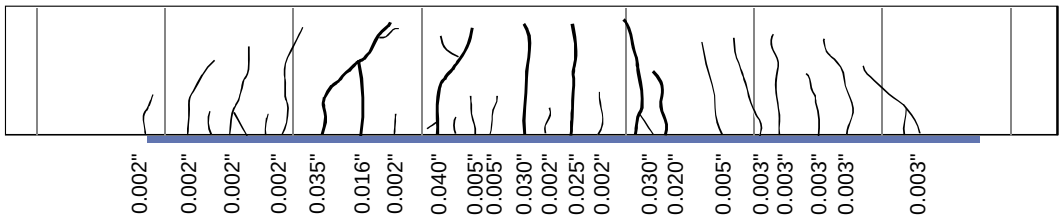

A3

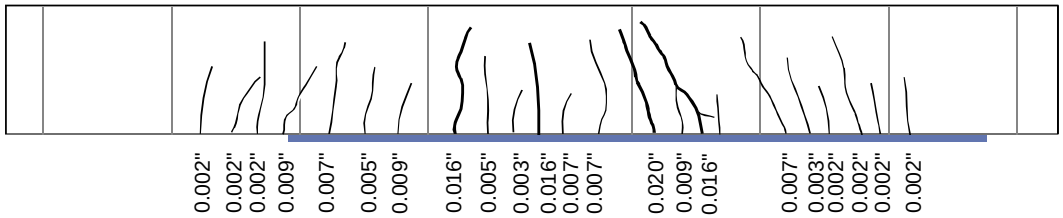
0.002"
0.002"
0.002"
0.009"
0.007"
0.005"
0.009"
0.016"
0.005"
0.003"
0.016"
0.007"
0.007"
0.020"
0.009"
0.016"
0.007"
0.003"
0.002"
0.002"
0.002"
0.002"

A4

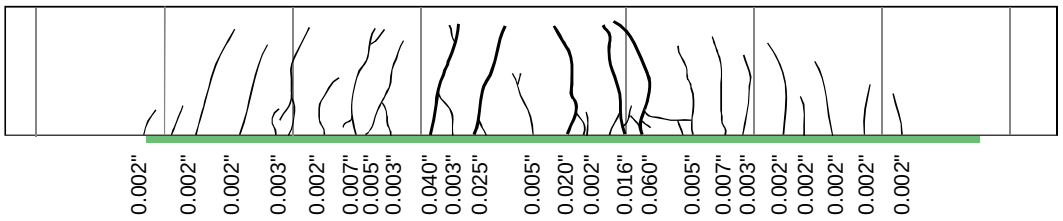
0.002"
0.002"
0.002"
0.003"
0.002"
0.007"
0.005"
0.003"
0.040"
0.003"
0.025"
0.005"
0.020"
0.002"
0.016"
0.060"
0.005"
0.007"
0.003"
0.002"
0.002"
0.002"
0.002"
0.002"

B1

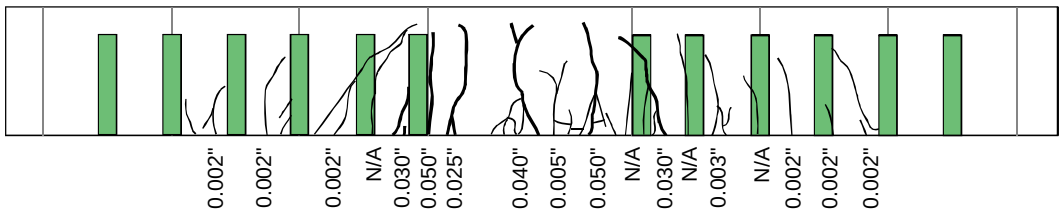
0.002"
0.002"
0.002"
N/A
0.030"
0.050"
0.025"
0.040"
0.005"
0.050"
N/A
0.030"
N/A
0.003"
N/A
0.002"
0.002"
0.002"

B2

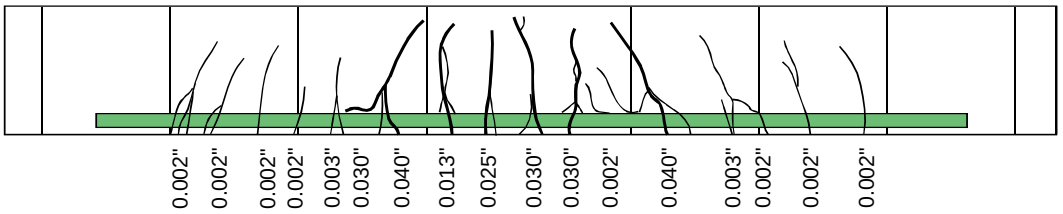
0.002"
0.002"
0.002"
0.002"
0.003"
0.030"
0.040"
0.013"
0.025"
0.030"
0.030"
0.002"
0.040"
0.003"
0.002"
0.002"
0.002"

B3

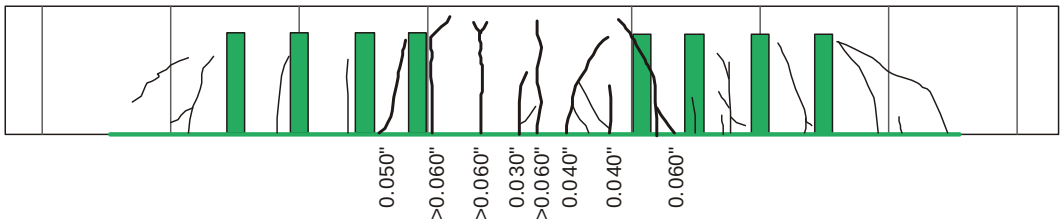
0.050"
>0.060"
>0.060"
0.030"
>0.060"
0.040"
0.040"
0.060"

B4

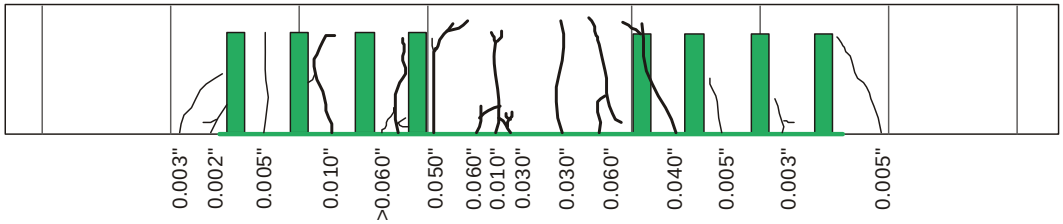
0.003"
0.002"
0.005"
0.010"
>0.060"
0.050"
0.060"
0.010"
0.030"
0.030"
0.060"
0.040"
0.005"
0.003"
0.005"

B5

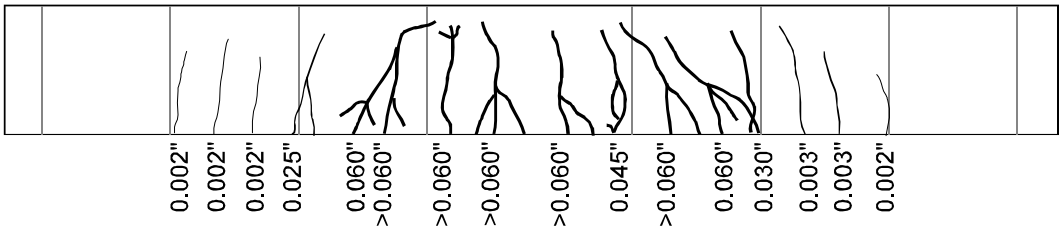

Control C & D

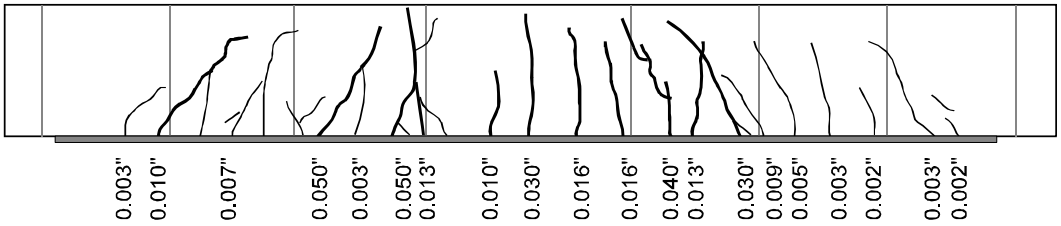

C1

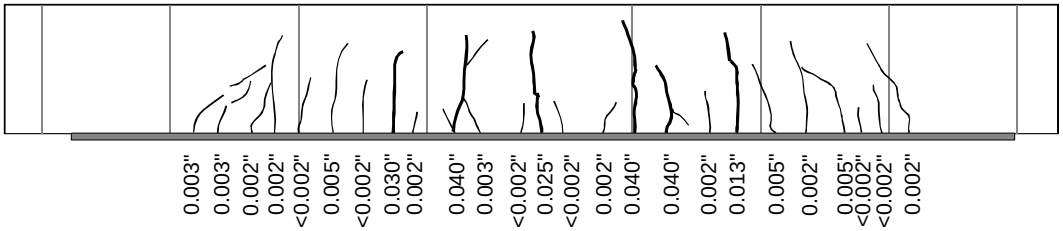

C2

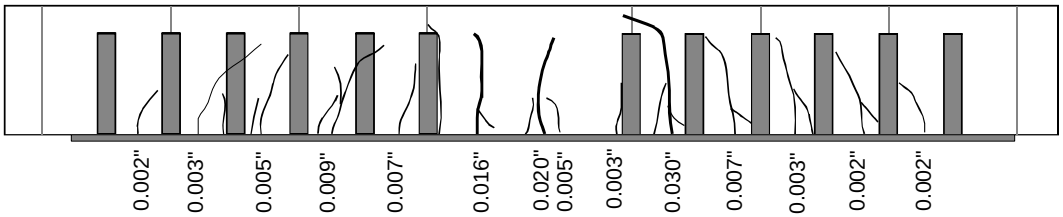

C3

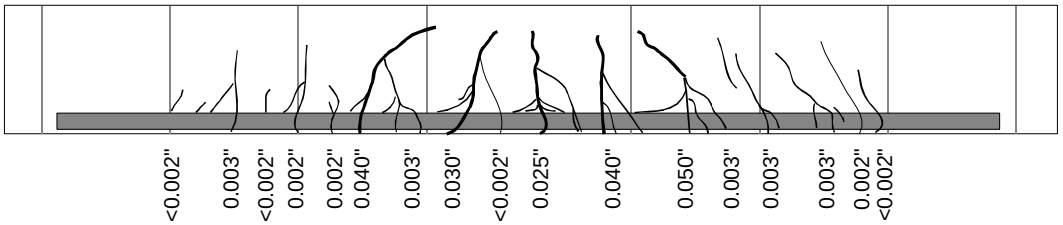
<0.002" 0.003" <0.002" 0.002" 0.002" 0.040" 0.003" 0.030" <0.002" 0.025" 0.040" 0.050" 0.003" 0.003" 0.003" 0.002" <0.002"

C4

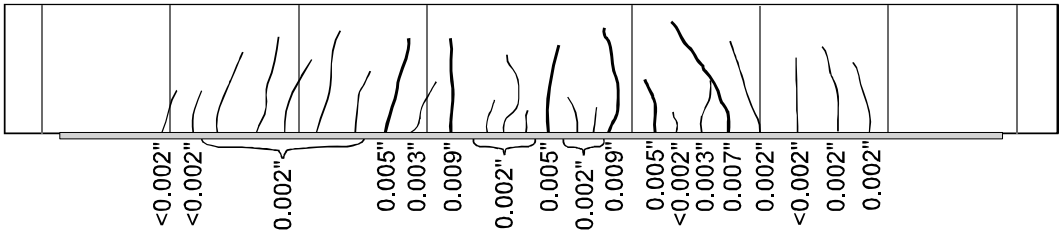
<0.002" <0.002" 0.002" 0.005" 0.003" 0.009" 0.002" 0.005" 0.002" 0.009" 0.005" <0.002" 0.003" 0.007" 0.002" <0.002" 0.002" 0.002"

D1

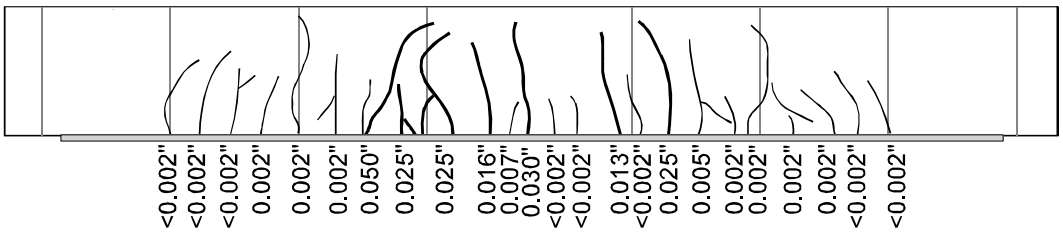
<0.002" <0.002" <0.002" 0.002" 0.002" 0.002" 0.050" 0.025" 0.025" 0.016" 0.007" 0.030" <0.002" <0.002" 0.013" <0.002" 0.025" 0.005" 0.002" 0.002" 0.002" 0.002" <0.002" <0.002"

D2

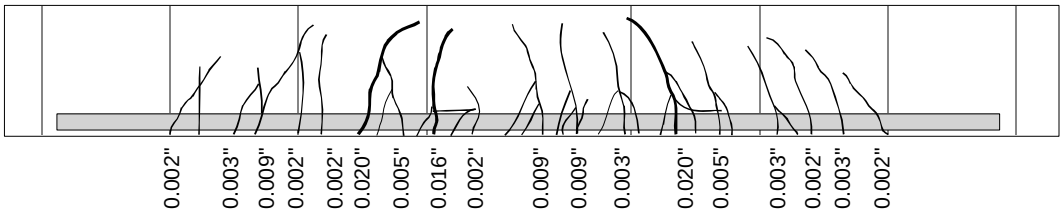
0.002" 0.003" 0.009" 0.002" 0.002" 0.020" 0.005" 0.016" 0.002" 0.009" 0.009" 0.003" 0.020" 0.005" 0.003" 0.002" 0.003" 0.002"

D3

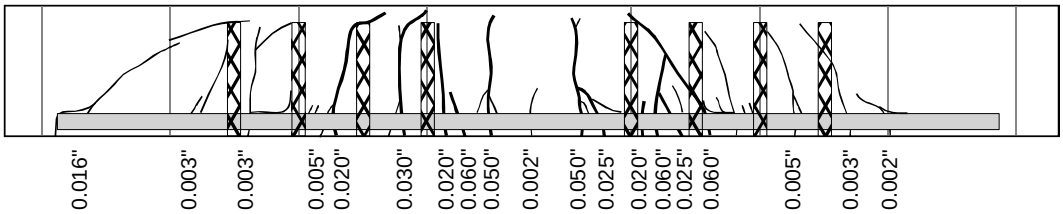
0.016"
0.003"
0.003"
0.005"
0.020"
0.030"
0.020"
0.060"
0.050"
0.002"
0.050"
0.025"
0.020"
0.060"
0.025"
0.060"
0.005"
0.003"
0.002"

D4

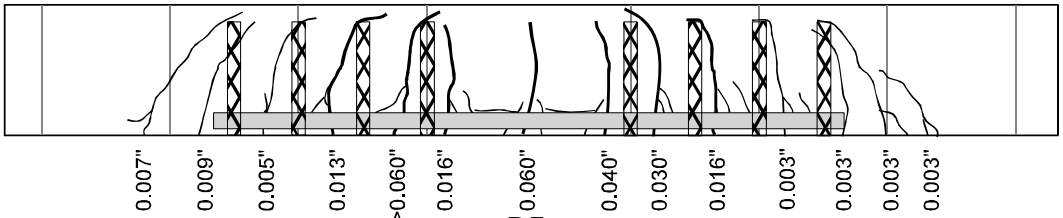
0.007"
0.009"
0.005"
0.013"
>0.060"
0.016"
0.060"
0.040"
0.030"
0.016"
0.003"
0.003"
0.003"
0.003"

D5

Appendix B: Strain Profiles at Critical Section

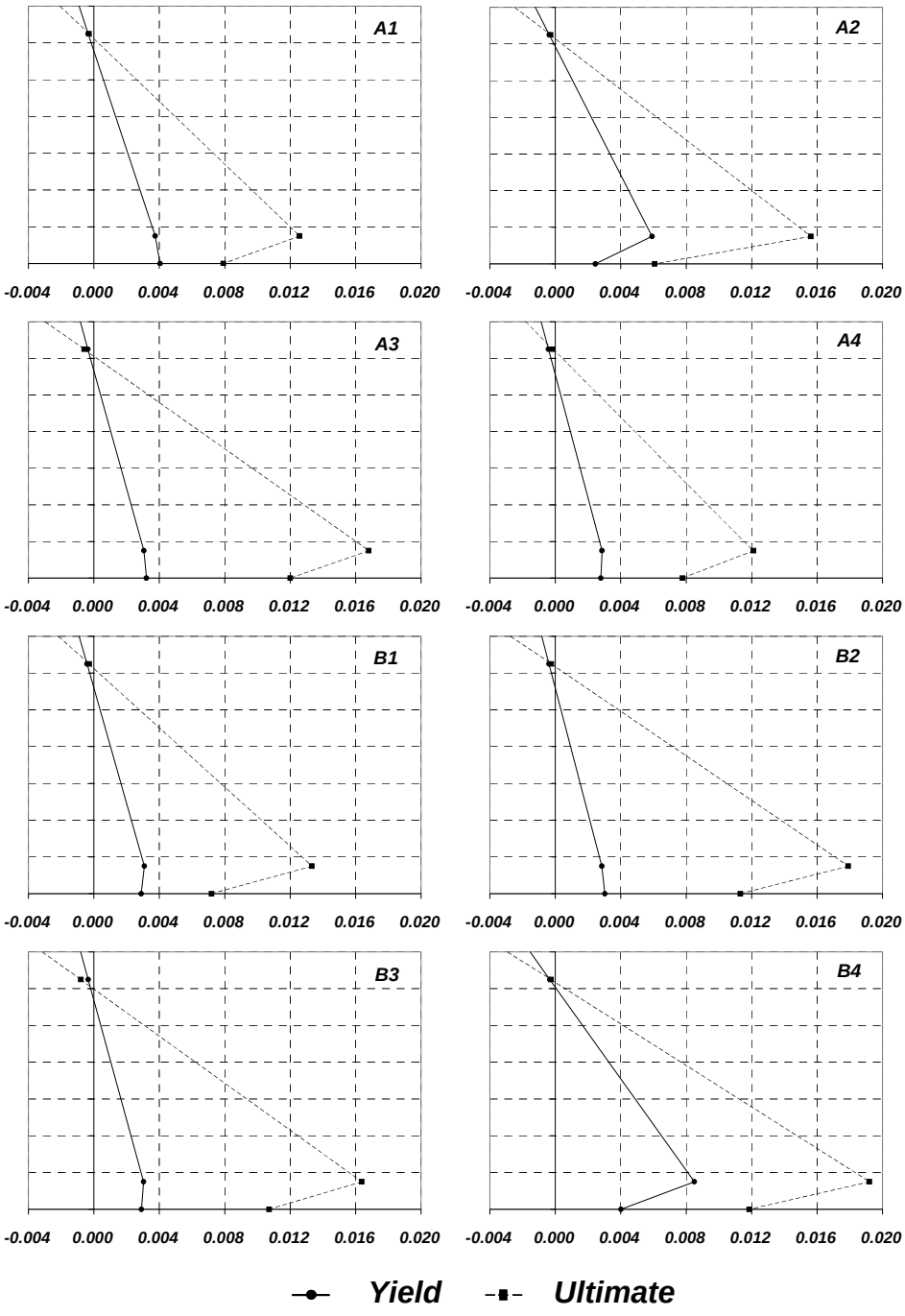

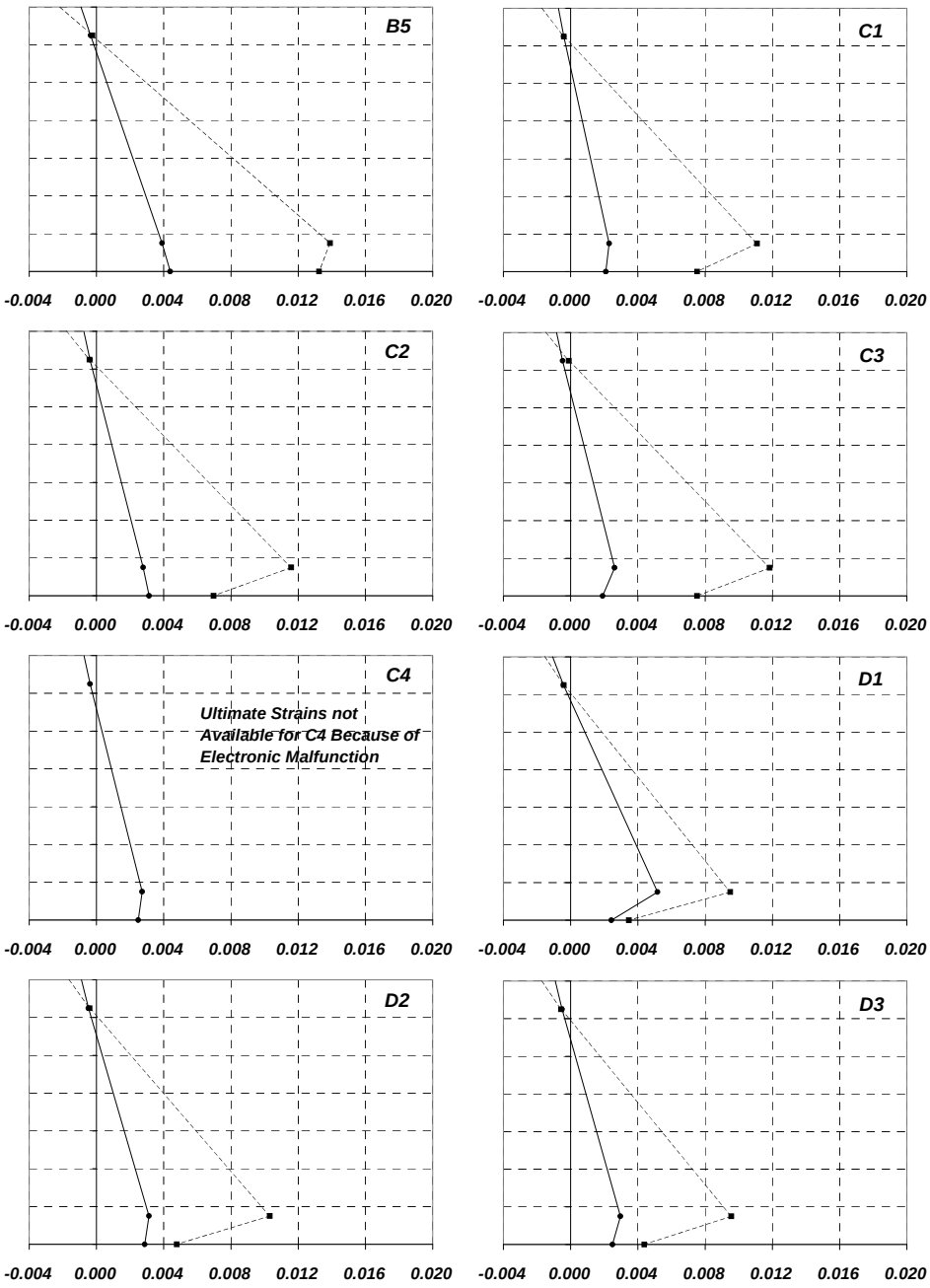
B5
C1
C2
C3
C4
Ultimate Strains not Available for C4 Because of Electronic Malfunction
D1
D2
D3
-0.004 0.000 0.004 0.008 0.012 0.016 0.020
Yield
Ultimate

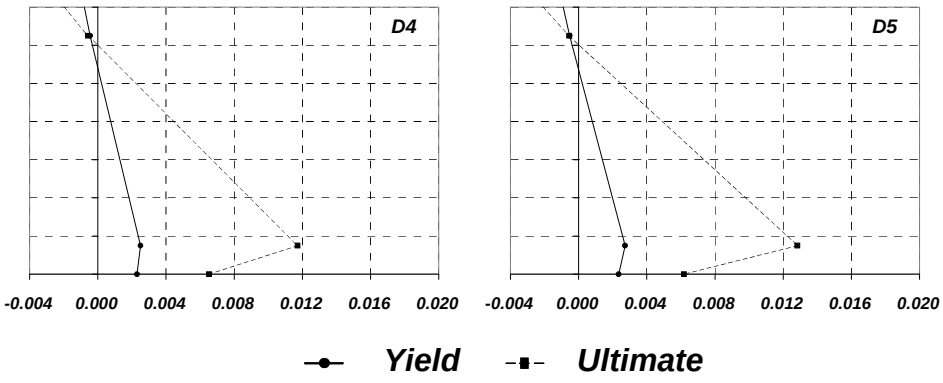
D4
D5
-0.004
0.000
0.004
0.008
0.012
0.016
0.020
Yield
Ultimate

References

Comment [slw1]: Please proof-read this section very carefully. There are many errors related to punctuation.

AASHTO, American Association of State Highway and Transportation Officials, *Standard Specifications for Highway Bridges, 16th Edition,* Washington D.C., 1996.

ACI Committee 343, "Analysis and Design of Reinforced Concrete Bridges Structures," (ACI 343R-88), *ACI Manual of Concrete Practice*, American Concrete Institute, Detroit, Michigan, USA, 1989, pp. 343R-1 to 343R-162.

Arduini A., Di Tommaso A., Manfroni O., Nanni A., "Failure Mechanisms of Concrete Beams Reinforced with FRP Flexible Sheets," *Proceeding of Advanced Composite Materials in Bridges and Structures, M.M. El-Badry, Editor*, Canadian Society for Civil Engineering, Montreal, Quebec, Canada, 1996, pp.253

Basset, Susan, "Carbon Laminates Solve Structural Problems in Bridges Across Continent." *High-Performance Composites*, March/April 1997, pp.22-27.

Berset J.D., "Strengthening of Reinforced Concrete Beams for Shear Using FRP Composites," *Massachusetts Institute of Technology, Master Thesis*, Cambridge, Massachusetts, USA, 1992.

BRINSAP, Texas Department of Transportation, Bridge Inventory, Inspection, and Appraisal Program Database, December 1998.

BRINSAP, Texas Department of Transportation, Bridge Inventory, Inspection, and Appraisal Program Group. Personal Communication, Fall 1997.

"Building Code Requirements for Structural Concrete (ACI 318-99) and Commentary (ACI 318R-95)," *American Concrete Institute,* 1999.

Cape Composites Incorporated, "Cape Composites: Carbon Fiber Data Sheet." Online. April 21, 2000. www.cape-composites.com/Pages/data.html

Curtis P.T., "The Fatigue Behavior of Fibrous Composite Materials," *Journal of Strain Analysis, Vol. 24, No.4*, 1989, pp.235-244.

Emmons P. H., Vaysburd A. M., Thomas J., "Strengthening Concrete Structures, Part I," *Concrete International*, March 1998, pp.53-58.

Emmons P. H., Vaysburd A. M., Thomas J., "Strengthening Concrete Structures, Part II," *Concrete International*, April 1998, pp.56-60.

FHWA, "The status of Nation's Highway Bridge Replacement and Rehabilitation Program and National Bridge Inventory," *Twelfth Report to the United States Congress*, US Department of Transportation, Federal Highway Administration, 1995.

FHWA, U.S. Department of Transportation Federal Highway Administration. "Table of Frequently Asked NBI Information Page." Online. July 7, 1999. www.fhwa.dot.gov/bridge/britab.htm

Ferguson, Phil M., Thompson, J. Neils, "Development Length of High Strength Reinforcing Bars in Bond," *ACI Journal, Proceedings Vol. 62, No. 7*, July 1962, pp. 887-992.

FYFE Co. LLC, "Design Manual for the TYFO Fibrwrap System", February 1998.

Gardens H.N., Hollaway L.C., "An Experimental Study of the Influence of End Plate Anchorage of Carbon Fiber Composite Plates Used to Strengthened Reinforced Concrete Beams", *Composite Structures 42*, 1998, pp. 175-188.

Gardens H.N., Quantrill R.J., Hollaway L.C., Thorne A.M., and Parke G.A.R., "An Experimental Study of the Anchorage Length of Carbon Fiber Composites Plates Used to Strengthened Reinforced Concrete Beams," *Construction Building Materials 12*, 1998, pp. 203-219.

Hognestad, Eivind, "A Study of Combined Bending and Axial load in Reinforced Concrete Members," *Bulletin 399*, University of Illinois Engineering Experiment Station, Urbana, IL, November 1951, pp.128.

Hognestad, Eivind, Hanson, N.W., McHenry, Douglas, "Concrete Stress Distribution in Ultimate Strength Design," *Journal of the American Concrete Institute, Vol. 52*, December 1955, pp. 455-479.

Hollaway L.C., Leeming M.B., "Strengthening of Reinforced Concrete Structures Using externally-Bonded FRP Composites in Structural and Civil

Engineering," *CRC Press, Woodhead Publishing Limited*, Cambridge, England, 1999, pp. 327.

Inoue S., Nishibayashi S., Kuroda T., Omata F., "Deformation Characteristics, Static and Fatigue Strengths of Reinforced Concrete Beams Reinforced with Carbon Fiber Reinforced Plastic Plate," *Transactions of the Japan Concrete Institute, Vol. 17*, 1995, pp. 149-156.

Inoue S., Nishibayashi S., Yoshino A., Omata F., "Deformation Characteristics, Static and Fatigue Strengths of Reinforced Concrete Beams Reinforced with Carbon Fiber Reinforced Plastic Plate," *Transactions of the Japan Concrete Institute, Vol. 18*, 1996, pp. 143-150.

MacGregor J. G., *Reinforced Concrete: Mechanics and Design*, Prentice Hall, New Jersey, Third Edition, 1998, p. 56.

Master Builders. "MBrace Composite Strengthening System." Online. August 2, 1999. www.mbrace.com

Master Builders, "MBrace® Composite Strengthening System Design Guide," *Master Builders*, 1998.

Meier U., Deuring M., Meier H., Schwegker G., " Strengthening of Structures with Advanced Composites," reprint from *Alternative Materials for the Reinforcement and Prestressing of Concrete*, 1993, pp.153-171.

Meier U., "Strengthening of Existing Structures Using Carbon Fiber/Epoxy Composites," *Construction and Building Materials*, Vol. 9 No. 6, 1995, pp. 341-351.

Meier, U., "Composites for Structural Repair and Retrofitting," *Proceeding of ICCI'96, Fiber Composite in Infrastructure*, 1996, pp. 1202-1216.

REPLARK, "Carbon Fiber Prepreg Sheet for Construction Industries", *Sumitomo Corporation of America*, November 1997.

Sika, "Sika CarboDur® Engineering Guideline for the Use of CarboDur® (CFRP) Laminates for Structural Strengthening of Concrete Structures," *Sika Corporation*, 1997.

Sika. "Sika.Com." Online. March 7, 2000. www.sikausa.com

Sika, “Strengthening of Structures with Carbon Fiber Reinforced Polymer Strips or Steel Plate,” *Sika Corporation*, 1999.

Spadea G., Bencardino F., Swamy R.N., “Structural Behavior of Composite RC Beams with Externally Bonded CFRP,” *Journal of Composites for Construction*, August 1998, pp. 132-137.

“Standard Specifications for Highway Bridges,” *AASHTO, sixteenth edition*, 1996.

Triantafillou, Thanasis C., “Shear Strengthening of Reinforced Concrete Beams Using Epoxy-Bonded FRP Composites,” *ACI Structural Journal*, March-April 1998, pp. 107-115.